Development of Advanced Solid-State Pulsed Lasers in the Near and Mid Infrared for Applications in Material Characterization

by

Hüseyin Çankaya

A Thesis Submitted to the
Graduate School of Engineering
in Partial Fulfillment of the Requirements for
the Degree of

Doctor of Philosophy
in
Materials Science and Engineering

Koç University

August 2011

Koç University

Graduate School of Sciences and Engineering

This is to certify that I have examined this copy of a doctor of philosophy thesis by

Hüseyin Çankaya

and have found that it is complete and satisfactory in all respects,
and that any and all revisions required by the final
examining committee have been made.

Committee Members:

_____

Alphan Sennaroğlu, Ph.D. (Advisor)

_____

Özgür Esat Müstecaplıoğlu, Ph. D.

_____

Havva Funda Yağcı Acar, Ph. D.

_____

Selçuk Aktürk, Ph. D.

_____

Alper Kiraz , Ph. D.

Date: _____

ÖZET

Bu doktora tezinde, darbeli yakın ve orta kızılaltı lazerlerin geliştirilmesi ve darbeli lazerlerin kuantum noktacıklarının optik özelliklerinin incelenmesi anlatılmıştır. Bilhassa bu tezde, femtosaniye ve pikosaniye Cr^{4+}:Forsterite lazeri, Nd katkılı tellürit cam lazeri ve sürekli dalga çekirdeklenen kazanç anahtarlamalı lazeri geliştirilmiştir. Ayrıca femtosaniye ve nanosaniye Ti:Safir lazerleri kullanılarak CdTe-CdS kuantum noktalarının iki foton soğurma özellikleri incelenmiştir.

Tezin ilk bölümde, düşük eşik gücü ile oda sıcaklığında çalışan kip kilitli Cr^{4+}:Forsterite lazerinin çalıştırılışı gösterilmiştir. Lazerin darbe tekrar frekansı, lazer kovuğuna çok yansımalı başka bir optik kovuk eklenerek 11.7 MHz'e düşürülmüştür. Lazeri darbeli çalıştırmak için Kerr odaklamalı kip kitleme yöntemi kullanılmıştır. Böylelikle lazerin çıkışından, sadece 60 mW ortalama güçle 5.1 nJ enerjili, 68 fs genişliğinde darbeler elde edilmiştir. Ayrıca 1.1 W soğrulmuş pompa gücü ile en düşük darbe genişli 41 fs olarak ölçülmüştür ve bu darbelerin enerjisi ise 3.4 nJ olarak belirlenmiştir.

Tezin ikinci bölümde ise, Cr^{4+}:Forsterite lazeri artı dispersiyon rejiminde çalıştırılmıştır. Bu rejimde, doğrudan bu lazerden şu ana kadar elde edilmiş en yüksek darbe enerji olan 81 nJ elde edilmiştir. Darbe tekrar frekansı ve genişliği sırasıyla 4.9 MHz ve 5.5 ps ölçülmüştür. Daha sonra lazer darbeleri, kovuk dışındaki kırınım ağları yardımı

ile 607 fs'ye sıkıştırılmıştır. Bu tayf bölgesinde çalışan, yüksek enerjili, kip kitli lazerlerin, derin doku çoklu foton mikroskopisi ve optik eş faz tomografisi gibi biyomedikal görüntüle sistemlerinde kullanılması beklenmektedir.

Tezin üçüncü bölümünde ise, $(0.8)TeO_2$-$(0.2)WO_3$ kompozisyona sahip Nd katkılı tellürit camlarından yapılan lazer gösterilmiştir. Bu çalışma, belirtilen kompozisyona sahip tellürit camlarından şu ana kadar elde edilmiş ilk lazer çalışmasıdır. Lazer, kazanç anahtarlama rejiminde, 114 μJ pompa enerjisi ile 1065 nm dalga boyunda 11 μJ'luk darbeler üretmektedir. Lazerin verim eğrisi yaklaşık % 12 olarak bulunmuştur. Daha sonrasında tellürit camı Nd iyonun diğer bir lazer geçişi olan $^4F_{3/2} \rightarrow {}^4I_{13/2}$ enerji geçişi kullanılarak 1370 nm'de çalıştırılmıştır. Bundan önce Nd katkılı tellürüt camlarından, bu dalga boyunda çalıştırılan başka bir lazer literatürde rapor edilmemiştir. Lazer 1 kHz tekrar frekansı ile 59 μJ darbe eşik enerjisi ile kazanç anahtarlamalı rejimde çalıştırılmıştır. Verim eğrisi yaklaşık % 5.5 olarak belirlenmiştir. Lazerden en yüksek 6 μJ darbe enerjisi elde edilmiştir. Bu darbelerin genişliği ise 1.74 μs olarak ölçülmüştür. Ayrıca eşik pompa enerjisi analizinden, camın ışıma arakesiti, uyarılmış seviye soğurması da dahil edilerek 1.57×10^{-20} cm^2 olarak hesaplanmıştır. Alınan sonuçlar, tellürit camlarının, cam ve fiber lazerinin geliştirilmesinde potansiyeli olduğunu göstermektedir.

Tezin dördüncü bölümünde ise 2255 ve 2455 nm aralığında dalga boyu ayarlanabilen, dar tayf genişliğine sahip kazanç anahtarlamalı Cr:ZnSe lazerin geliştirilmesi anlatılmıştır. Lazerin tayf genişliği, optik tohumlama yöntemi kullanılarak

125 nm'den 0.65 nm'ye düşürülmüştür. Tohumlama sırasında başka bir dalga boyu ayarlanabilen sürekli dalga Cr:ZnSe lazeri kullanılmıştır. Darbeli lazerin dalga boyu sürekli lazerin dalga boyu değiştirilerek kontrol edilmiştir. Darbeli lazerden en yüksek 157 μJ darbe enerjisi elde edilmiştir. Bu sırada pompa darbe enerjisi 598 μJ ve darbe tekrar frekansı 1 kHz'dır.

Tezin son bölümünde ise darbeli Ti:safir lazeri kullanılarak CdTe-CdS kuantum noktalarının iki foton soğurma ve sonucunda oluşan ışıma özellikleri incelenmiştir. Ayrıca kuantum noktalarının ışıma güçlerinin 740-860 nm uyarma dalga boyu aralığında değişmediği gösterilmiştir. Işıma veriminin ise Rodamin 6G'ye % 60.7 olduğu belirlenmiştir. Ayrıca iki foton soğurma ara kesiti 4.1×10^6 GM olarak bulunmuştur.

ABSTRACT

This thesis investigates the experimental development of novel advanced pulsed lasers in the near and mid infrared and use of pulsed lasers in the optical characterization of quantum dots. In particular, the development of solitary and chirped-pulse Cr^{4+}:Forsterite laser, Nd doped tellurite glass laser and continuous-wave injection-seeded gain-switched Cr:ZnSe laser was investigated. In the second part, pulsed Ti:sapphire lasers operated in the nanosecond and femtosecond regimes were used to measure the two-photon absorption characteristics of CdTe-CdS quantum dots.

The first part of the thesis focuses on the experimental demonstration of a mode-locked, low-threshold, room-temperature, multipass-cavity femtosecond Cr^{4+}:Forsterite laser. The repetition rate was lowered to 11.7 MHz by introducing a q-preserving multipass cavity. Pulse formation could be achieved by using the Kerr-lens mode-locking technique. Nearly transform-limited 5.1-nJ pulses with a duration of 68 fs were generated at an output power of only 60 mW. Furthermore, as short as 41-fs pulses could be obtained with a pulse energy of 3.4 nJ at an absorbed pump power of only 1.1 W.

In the second part of the thesis, the Cr^{4+}:Forsterite laser was operated in the positive dispersion regime. We obtained record 81-nJ pulses directly from the Cr^{4+}:Forsterite oscillator at a pulse repetition rate of 4.9 MHz. In that case, pulse duration at the output was 5.5 ps. By using an external grating compressor , the pulses were then compressed to

607 fs. High-energy mode-locked oscillators operating in this wavelength range should be important in various biomedical applications including deep-tissue multi-photon microscopy as well optical coherence tomography.

In the third part, lasing action in a novel, neodymium-doped tellurite-based glass with the host composition $(0.8)TeO_2$-$(0.2)WO_3$ was demonstrated. To our best knowledge, this is the first time laser operation from Nd:Tellurite glass with this composition was reported in the literature. During gain switched operation, the glass laser produced 11 μJ of output energy at 1065 nm with 114 μJ of pump energy. The slope efficiency with respect to the incident energy was 12%. Then, the laser was operated at 1370 nm by using the other laser transition of the Nd^{3+} ion . To our best knowledge, lasing action at 1370 nm was demonstrated for the first time in a bulk tellurite glass host for the energy transition $^4F_{3/2} \rightarrow {}^4I_{13/2}$ of the Nd^{3+} ion. The laser was operated in gain-switched regime at 1 kHz with a threshold pulse energy of 59 μJ. The slope efficiency was further determined to be 5.5 %. As high as 6μJ-pulses with a duration of 1.74 μs were obtained. From the threshold analysis, the emission cross section came to 1.57×10^{-20} cm^2 in the presence of excited-state absorption. These results indicate that doped tellurite glasses have the potential of being used in the development of efficient bulk glass lasers and fiber lasers in the near infrared.

In the fourth part of the thesis, we reported a narrow-linewidth, tunable, gain-switched Cr:ZnSe laser operating between 2255 and 2455 nm. The spectral width of the

laser was reduced from 125 nm to 0.65 nm by using injection seeding. Seeding was achieved with another tunable, continuous-wave Cr:ZnSe laser. The wavelength of the laser was controlled by tuning the wavelength of the seed laser. The seeded gain-switched oscillator produced as high as 157 μJ-pulses with 598 μJ incident pump pulse energy at a repetition rate of 1 kHz.

Finally, we demonstrated an application of pulsed Ti:sapphire lasers in the optical characterization of quantum dots. By using pulse lasers, we analyzed the two-photon absorption and resulting emission of core-shell CdTe-CdS q-dots. We showed that emission strength of the sample was independent of the wavelength of the pump laser in the range of 740-860 nm. Moreover, we found out the luminescence efficiency to be 60.7 % with respect to Rodamin 6G. Furthermore, the two-photon absorption cross-section was determined to be 4.1×10^6 GM.

ACKNOWLEDGEMENTS

This thesis will be on “Development of advanced near and mid-infrared pulse lasers and an application in optical characterization of quantum dots”. As my work for a PhD degree at Koc University ends, I would like to thank all the people that have provided me technical, economical and non-technical support.

First and foremost, I would like to thank my thesis advisor Prof. Alphan Sennaroglu for all the guidance and technical support during these years. He has been a great advisor beginning from my undergraduate years up to the end of my PhD. I learned from him not only the technical information but also understanding of research. I would also like to thank Adnan Kurt for his constant involvement with my research at KU and his personal support in hard times. My interaction with Prof. Sennaroglu and Adnan Kurt has provided me a great opportunity to gain not only experience in experimental research but also non-technical skills.

Dr. Hamit Kalaycioglu has also contributed significantly to the glass laser project and I would like to thank for their continuing support and also friendship during my Ms and PhD years. Without his support it was impossible to complete this project. I would like to thank to M. Natali Cizmeciyan about her contribution in this thesis. We overcame many problems in laboratory together. During these years, I have enjoyed interacting with the student members of KU LRL group, Adil Tolga Gorgulu, Ersen Beyatli, Solmaz Nazghizadeh, Isinsu Baylam and former members Dr. Umit Demirbas, Sehat Tozburun, Ahmet Koray Erdamar and Reyhane Kilci.

I would like to also acknowledge to the collaborators from Istanbul Technical University, Prof. Gonul Ozen, Prof. M.Lutfu Ovecoglu, and Prof. Selcuk Akturk. Especially, Prof. Ovecoglu and Prof. Ozen guided me in preparation of the glass samples

used in the experiments as well as courses I took. Prof. Selcuk Akturk contributed in chirped-pulse Cr^{4+}:Forsterite project.

I would like to thank to Esra Sevinc and her advisor Prof. Funda Havva Yagci Acar about their contributions in quantum dot analysis. They contributed to this thesis by preparing excellent quality quantum dot samples.

I would also like to thank my PhD. supervision committee member Prof. Ozgur Esat Mustecaplioglu for his continuous involvement and helpful comments during my presentations. I would like to also thank to Prof. Alper Kiraz for taking his valuable time to serve on my thesis committee.

The primary support for my studies was provided by KU and TÜBITAK. I am grateful for their support without which this work would not have been possible.

Finally, I wish to thank my parents for their continuing support and love during my entire time at KU.

This thesis is dedicated to the love of my life, my wife, Zeynep, for her endless love and support.

TABLE OF CONTENTS

LIST OF TABLES

LIST OF FIGURES

NOMENCLATURE

c	speed of light
L_c	length of the laser cavity
$(\mathrm{E_p})_{\mathrm{in}}$	intracavity pulse energy
D	net group delay dispersion of the cavity
δ	Kerr coefficient
τ	pulse duration divided by 1.76
M_t	ray transformation matrix
A, B, C, D	elements of the ray transformation matrix
θ	angular rotation of the spot after one round trip
n	number of full round trips of photons in a multipass cavity
m	number of semicircular arcs of photons in a multipass cavity
R	radius of curvature of a curved mirror
L	distance between two multipass cavity
τ_p	laser pulsewidth
λ_L	wavelength of the laser
λ_p	wavelength of the pump laser
$\Delta\lambda$	spectral width of the laser FWHM
L_r	roundtrip loss of the cavity
T	transmission of the output coupler
σ_L	stimulated emission cross section of the gain medium
E_{th}	incident threshold pulse energy
h	Planck's constant
hv_p	pump photon energy

w_L	laser spotsize inside the gain medium
w_P	pump laser spotsize inside the gain medium
$w(z)$	laser spotsize function
w_{rms}	root mean square of spotsize function
η_a	absorption of the gain medium at the pump wavelength
σ_{ESA}	excited state absorption cross section at laser wavelength
T_{opt}	optimum transmission of the output coupler
E_p	output pulse energy
r	ratio of maximum available pump pulse energy to the threshold pulse energy
τ_f	fluorescence lifetime of the upper energy level
f_L	ratio of the excited state absorption cross section to the emission cross section
η	slope efficiency of the laser
L_0	length of the gain medium
σ_{TPA}	two-photon absorption cross-section
β	two-photon absorption coefficient
I_p	pump photon intesity
ρ	Maxwell-Garnet local field correction factor
N	quantum dot concentration

Chapter 1

INTRODUCTION

This thesis is focused on the development of pulse laser sources operating in the near and mid-infrared spectral regions for various applications including medical imaging, remote gas sensing and materials characterization. At the end of the thesis, two-photon absorption-induced emission properties of quantum dots will be characterized as a representative application of such lasers. In this chapter, a general overview of laser technology will be provided to make the reader familiar with the basic concepts and then an outline of the thesis will be presented.

1.1 An Overview of Laser Technology

Laser is the acronym for "Light Amplification by Stimulated Emission of Radiation". Even though the meaning of the acronym is a description of a process, it stands for a device. The first laser was a pulsed ruby laser invented by Theodore Maiman in 1960 [1] in the light of pioneering works of Arthur Schawlow, Charles Hard Townes, Nikolay Basov and Alexander Prokhorov. The invention of the laser initiated many fields in optics. A few of them are fiber optics technology [2], optical clocks [3], photonic crystals [4-5], and

multiphoton microscopy [6]. The unique optical properties of the laser light make the laser a key component in photonics. Some of these properties can be listed as follows:

- It can propagate over a long distance without much spreading at the diffraction limit.
- It can have a very high spectral grightness since its emission linewidth is much narrower than common sources of light such as light bulbs or light emitting diodes.
- It can be emitted continuously or in pulse regime with pulse duration in the range of microseconds to a few femtoseconds.

Lasers can be categorized into three main groups (gas, liquid and solid-state lasers) with respect to the physical characteristics of their gain media. Gas lasers have relatively high gain in comparison with solid-state lasers that allows kW levels of continuous-wave output power and kJ level of pulse energy [7]. Lasing transitions of gas lasers are relatively narrow. However, a gas laser can operate in many distinct transitions at the same time without introducing any tuning element into the cavity [7-8]. Nowadays, the solid-state lasers are replacing the gas lasers operating in the visible to mid-infrared spectral regions due to high stability and robustness.

Liquid laser gain media are based mostly on organic dye molecules. With respect gas laser transitions, dye molecules have large spectral bandwidths that enable tuning of the laser as well as femtosecond pulse generation [9]. In addition, the emission cross section of

dye molecules are higher than those of most solid-state gain media. Furthermore, the upper state lifetime is in the ns levels that enables stable mode-locked operation without q-switching instabilities [10]. Unfortunately, dye molecules are very impractical because of their highly toxic and corrosive nature [7]. The other disadvantages of liquid lasers are the low output powers and the requirement for expensive pump sources [10]. Because of this,nowadays, liquid lasers are being replaced by solid-state counterparts.

Solid-state lasers are based on ion doped solid gain media including single crystals, ceramics, and glasses. Even though semiconductor lasers have solid-state gain medium, they can be classified in a new category because the physical mechanism behind generation of light is completely different from the other laser systems [7]. In semiconductor lasers, population inversion is obtained by creating electron hole pairs. However in the solid-state lasers, the population inversion is generated by exciting the active ions to upper energy state. In addition, the operation wavelength of the semiconductor laser can be controlled by tailoring the band gap of the semiconductor. Furthermore, the semiconductor lasers are generally electrically excited. There are also semiconductor lasers pumped optically such as optically pumped VECSEL's (Vertical-external-cavity surface emitting lasers) [11]. Except for color-center laser media, most solid-state laser materials have relatively low emission cross section in comparison withgas and liquid lasers. However, they are chemically and mechanically very robust and stable systems. Furthermore, they have excellent beam quality in general. There are various types of solid-state lasers including

fiber lasers [12-14], waveguide lasers [15-16], slab lasers [17-19], thin disk lasers [20-21], bulk glass [22-25] and crystalline lasers [26-28]. In this thesis, we will be mainly focused on bulk crystalline and glass laser development.

1.2 Different Modes of Operation for Solid-State Lasers

Depending on the temporal characteristics of the output, lasers can be classified into two groups: continuous-wave (cw) and pulsed lasers. The output power of a continuous-wave laser is almost constant with respect to time. In continuous-wave lasers, several longitudinal modes oscillate at the same time, leading to beatingamong the field components atslightly different optical frequencies. That leads to a small modulations in the output of the laser in time scales shorter than the round-trip time of the laser resonator. However on average, the output power remains constant over long time scales.

In pulsed lasers, the output varies as a function of time. This temporal variation is in addition to the oscillation taking place at the carrier frequency which is typically very high (100-500 THz). There are three methods, namely q-switching, gain-switching and mode-locking, to produce pulsed laser output. In q-switching technique, the quality factor (q-factor) of the optical resonator switches between high and low levels by using an intracavity optical modulator. In other words, the switch controls the loss of the cavity. When the q-factor of the resonator is low (corresponding to high loss in the cavity), the population in the upper-state increases. When the q-factor is increased (low loss in the

cavity), the population in the upper energy level is depleted via stimulated emission that results in the production of a short giant pulse from the output of the laser. By using the q-switching technique, it is possible to produce pulses with gigawatt peak powers [29]. However the pulsewidths are typically in the range of nanoseconds, the exact duration depending on the length and passive loss of the cavity.

In the gain-switched lasers, the pump source is itself a pulsed laser. In this method, the duration of the pulses are directly dependent on the pump pulsewidth. We employed the gain-switching technique in Nd doped tellurite glass and Cr:ZnSe lasers which will be described in Chapters 4 and 5, respectively. Some applications (such as remote gas sensing [30]) requires narrow bandwidth laser sources. One of the issues to be addressed in gain-switched lasers with large gain bandwidth is the broad spectral width of the laser output. Mode-locked lasers also have broad spectrum but the phases of the oscillating modes supported by the resonator are locked, allowing much shorter pulses in the picosecond and femtosecond time scales [31]. However in gain-switched lasers, the pulsewidths are in the ns range. In broad-bandwidth, gain-switched lasers, the spectral width of the output can be reduced by either introducing a wavelength selective element [32] or seeding the laser with a narrow-bandwidth laser source [33]. We preferred the seeding method to narrow the spectrum of the gain-switched Cr:ZnSe laser in our experiments. Why we choose the second method will be described in Chapter 5.

In mode-locked lasers, the phases of the allowed longitudinal cavity modes supported by the gain media are locked by using a fast optic switch inside the cavity. Interference between these modes leads to a pulse train at a repetition rate given by $c/2\,L_c$ where c is the speed of light and L_c is the effective optical length of the cavity. The duration of the pulses is inversely proportional to the number of locked modes. By using this method, pulses with few femtosecond duration were reported [31, 34]. In mode-locked lasers, the phase of the modes can be locked by using an active or a passive optic switch. Nowadays, passively mode-locked systems are preferred because of the fact that pulsewidths in actively mode-locked lasers tend to be much longer (on the order of picoseconds). In passively mode-locked systems, either semiconductor saturable absorber mirrors (SESAM's) [35] or the gain medium itself can be used as the optical modulator. SESAM is a device which has an intensity dependent reflection. As the intensity of the light incident on the SESAM is increased, its reflectivity also increases. In a continuous-wave laser, random amplitude fluctuations are present, as mentioned before. When a SESAM is introduced into the cavity of a continuous-wave laser, the intense spikes will be selectively reflected by the SESAM and amplified in the gain medium. That leads to the oscillation of only the intense spikes which can be attained when the longitudinal modes are locked in phase. After many round-trips, that results in the formation of a mode-locked pulse train [35].

Mode-locked lasers in which gain medium is used as the optical switch is called Kerr-lens mode-locked (KLM) lasers. In these lasers, the Kerr effect is the main mechanism behind mode-locking. Kerr effect is a nonlinear effect where the refractive index of the medium becomes a function of the light intensity. If the Kerr coefficient of a medium is positive, the refractive index increases as a function of intensity. When a Gaussian beam is focused inside a medium with positive Kerr nonlinear coefficient, the refractive index gradient induced by Kerr effect leads to lensing and can cause self focusing. In KLM lasers, the pump spot is chosen to be smaller than the spot size of the laser inside the gain medium. With an intense spike inside the gain medium, the laser light undergoes self focusing and overlaps more effectively with the pump spot. Since the mode-matching between the pump and the laser beam is increased, only the high intensity mode can survive in the cavity and the laser automatically starts to operate in the mode-locked regime. Note that the intracavity intensity of mode-locked lasers is typically much higher than in continuous-wave lasers. In KLM lasers, mode-locking is commonly initiated with a mechanical perturbation, as, for example, by moving one of the end mirrors. The main advantage of KLM lasers is that there is no need for an additional optical switch. As described in Chapters 2 and 3, Kerr-lens mode-locking technique was employed to obtain femtosecond pulses from a Cr:forsterite laser.

In mode-locked lasers, the group delay dispersion (GDD) of the cavity is an important parameter that determines the steady-state pulse duration. When the total GDD

of the cavity is negative, the nonlinear phase shift originating from the Kerr effect is compensated,resulting in solitary pulses whose duration is determined by the available gain bandwidth. This is typically in the picosecond or femtosecond regime. The relationship between dispersion and pulsewidth is given by the soliton area theorem: [36],

$$\left(E_p\right)_{in} = \frac{4|D|}{\delta\tau}. \tag{1.1}$$

Here, $\left(E_p\right)_{in}$ is the intracavity pulse energy, D is the net GDD of the cavity, δ is the Kerr coefficient and τ is the pulse duration (FWHM) divided by 1.76. In a mode-locked laser, it is possible to increase the pulse energy simply by increasing the cavity length, provided that the average output power remains the same. However, to maintain the same pulsewidth as this is done, it is necessary to increase the amount of negative GDD as can be seen from Eq. (1.1). One of the most challenging issues in high energy femtosecond laser development is the management of hig levels of GDD inside the cavity without introducing extra losses. This can be done by using double-chirped mirrors (DCM's) [37] or Gires–Tournois interferometer (GTI) mirrors [38]. However these mirrors are not commercially available for all the spectral ranges. Furthermore, the current coating technologies are not able to produce GDD levels comparable to what can be obtained with diffraction gratings. Mirrors for non-standard spectral ranges such as the mid infrared require special designs which considerably increase the cost of the laser system. Another alternative for this problem can be mode-locked operation in the positive dispersion regime where a relatively

small amount of net positive intracavity dispersion combined with KLM can also produce high-energy, chirped pulses in the picosecond time scales. The residual chirp of the output pulses can then be removed externally by using a prism or a grating pair [39-43]. Another important advantage of chirped-pulse oscillation is that the damage risk of various intracavity elements is significantly reduced due to lower peak powers inside the cavity. In our experiments, we operated a Cr^{4+}:Forsterite laser in both of these mode locking regimes: solitary pulse formation and chirped pulse formation. The details of the experiments will be discussed in Chapters 2 and 3.

1.3 Overview of Thesis

This thesis is focused on development of advanced near and mid-infrared pulsed lasers and their application in optical characterization of quantum dots. In particular, the thesis consists of the development of a solitary and chirped-pulse Cr^{4+}:Forsterite laser, Nd doped tellurite glass laser, continuous-wave injection-seeded gain-switched Cr:ZnSe laser and optical characterization of CdTe-CdS quantum dots. In Chapter 2, we will present an efficient multipass-cavity femtosecond Cr^{4+}:Forsterite laser at the wavelength around 1270 nm. The laser was operated in the negative dispersion regime. Then, in Chapter 3, the laser was operated in positive dispersion regime where the laser produced chirped pulses with picosecond duration. The results and the advantages of chirped oscillation will be discussed. In Chapter 4, we will describe the gain-switched operation of a Nd doped

tellurite glass laser at the wavelengths of 1065 nm and 1370 nm. Chapter 5 will discuss an efficient continuous-wave injection-seeeded pulsed Cr:ZnSe laser operating in the mid-infrared spectral region. Finally, in Chapter 6, we will demonstrate an application of pulsed lasers in the characterization of two-photon absorption properties of CdTe-CdS quantum dots. At the beginning of each Chapter, a brief motivation behind the experiments and a literature review of the particular topic will be provided.

Chapter 2

SOLITARY PULSE GENERATION WITH A MULTIPASS CAVITY Cr^{4+}:FORSTERITE LASER

2.1 Introduction

There is a growing demand for high energy, femtosecond lasers in diverse applications including medical imaging [44], high harmonic generation [45], and inner-shell spectroscopy [46] to name a few. The peak power of the laser pulses can be increased by employing different approaches, such as scaling up the pump power or using an external amplifier system. However, these methods also lead to a significant increase in the overall cost because additional pump lasers and optical components are required. An alternative solution involves lowering of the pulse repetition rate by increasing the length of the cavity. If the average output power of the femtosecond oscillator remains the same, increasing the overall cavity length scales up the pulse energy proportionally. The major drawback of this approach is that the long-cavity laser is difficult to construct in practice. Furthermore, the addition of the long cavity will in general change the q-parameter of the short cavity and modify the operating point during Kerr-lens mode locking (KLM). This drawback can be

obviated by using Herriot multipass cavities (MPC) which provide long effective optical paths lengths in a compact geometry [47]. The use of MPC's inside femtosecond lasers was first utilized by Cho *et al.* [48] who reported the generation of 16.5fs, 11 nJ pulses from a Ti:sapphire laser. Typically, it is desirable to use a q-preserving MPC [49] which leaves invariant the original spotsize distribution inside the short cavity. Once the q-preserving MPC is added to the short cavity, high-energy femtosecond pulses can be obtained with relatively low average output powers and low pump powers. To date, this technique has been applied to a wide range of lasers including Ti:sapphire [50-51], Yb:YAG [21], Cr:LiSAF [52], and Nd:Vanadate [53-54].

In this part of the thesis, we focus on the design and experimental demonstration of a efficient multipass-cavity femtosecond Cr^{4+}:Forsterite laser operating near 1270 nm. First, we briefly review the design principles of q-preserving multipass cavities. Second, we describe the experimental setup and present data showing the continuous-wave power performance of the short and extended cavities. During mode-locked operation, we obtained 4 nJ of pulse energy at an average output power of only 47 mW. The corresponding absorbed pump power during mode-locked operation was 1250 mW. With the addition of the MPC, the laser operated at a repetition rate of 11.7 MHz. The output pulsewidth and spectral bandwidth were measured to be 90 fs and 23 nm, respectively, corresponding to a time-bandwidth product of 0.37. The obtained results were presented in Advanced Solid-State Photonics (ASSP) 2009 [55].

2.2 Design of the Multipass Cavity

In this section, we review the basic design rules of the q-preserving multipass cavity [49, 56]. In the determination of the multipass-cavity parameters, we can employ the standard ABCD matrix method. If A, B, C, and D are the elements of the round-trip ray transformation matrix M_T, the transformation matrix for n full round trips through the MPC becomes

$$M_T^{\,n} = \begin{bmatrix} \dfrac{(A-D)\sin n\theta}{2\sin\theta} + \cos n\theta & B\dfrac{\sin n\theta}{\sin\theta} \\ C\dfrac{\sin n\theta}{\sin\theta} & \dfrac{(D-A)\sin n\theta}{2\sin\theta} + \cos n\theta \end{bmatrix}. \tag{2.1}$$

When the offset and angular inclination of the incident beam are properly adjusted, the bouncing beam forms a circular spot pattern on each mirror. In this case, the angle θ corresponds to the angular rotation of the spot after one round trip [49]. For the MPC to be q-preserving after *n* full round trips, $M_T^{\,n}$ should be equal to $\pm I$, where *I* is the identity matrix. In this case, the angular rotation θ satisfies the simple condition

$$n\theta = m\pi . \tag{2.2}$$

Here, *n* represents the number of full round trips and *m* represents the number of semicircular arcs that the bouncing beam completes before exiting the multipass cavity. In our particular design, the MPC consisted of a flat and a curved (radius of curvature=*R*) notched high reflector. In this case, the separation distance *L* between the mirrors for *q* preserving configurations is given by [56]

$$L = \frac{R\left(1-\cos\left(\frac{m\pi}{n}\right)\right)}{2}. \qquad (2.3)$$

2.3 Experimental

Figure 2.1 shows a schematic and photograph of the experimental setup for the short and the extended-cavity Cr^{4+}:Forsterite laser. The short cavity which operated at a repetition rate of 195 MHz had a standard astigmatically-compensated x-configuration with two highly reflecting curved mirrors each with a radius of curvature of 5 cm (M1 & M2) and two flat mirrors (M3 & OC). We used two different output couplers having transmission of 2.5 and 4.7 % at 1250 nm. The curved mirrors, M1 and M2, were separated by approximately 5 cm from each other. The high reflector and output coupler arm lengths were 42 and 30 cm, respectively. The resonator was end pumped by a continuous-wave Yb:fiber laser at 1060 nm. The pump laser was focused inside the 3-mm-long, Brewster-angled Cr^{4+}:Forsterite crystal by using a lens (L) with a focal length of 10 cm. The crystal was positioned near the center of the curved mirrors. The crystal was further wrapped in a thin indium foil and clamped inside a copper block maintained at room temperature (20 ºC) by water cooling. The absorption coefficient of the crystal was 1.75 cm^{-1}, corresponding to a total absorption of 41 %. The laser could be operated with absorbed threshold pump powers as low as about 290 mW at the output coupling level of 2.5 %, which is the lowest reported threshold value for this laser system at room temperature [57]. By measuring the

output power as a function of the incident pump power, the continuous-wave power slope efficiency was determined to be 6.3 and 5.9 % for 2.5 and 4.7 % output couplers, respectively (See Figure 2.2). The single-pass loss of the 195-MHz-short-cavity was further determined to be 1.7 % by measuring the threshold pump power at different output coupling levels.

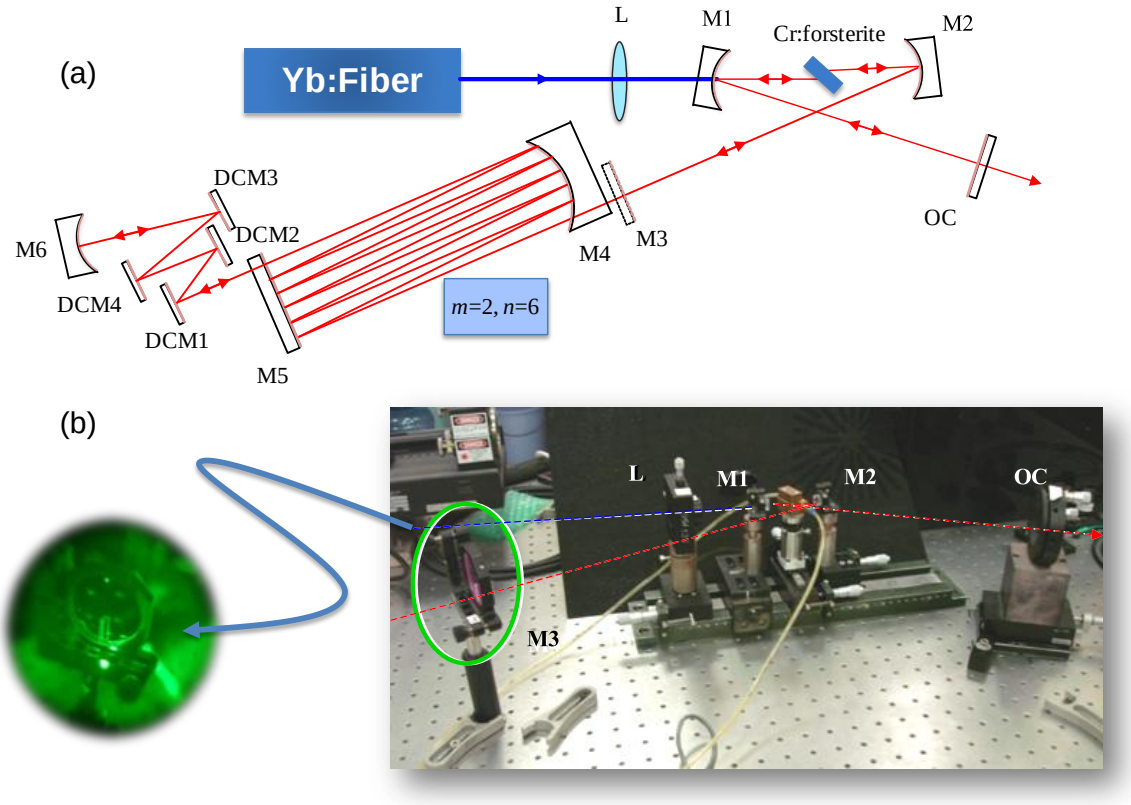

Figure 2.1: Schematic (a) and the picture (b) of the femtosecond multipass cavity (MPC) Cr^{4+}:Forsterite laser.

To scale up the pulse energy, the high reflector M3 was removed and the cavity length was increased by the addition of a flat-curved q-preserving MPC. MPC provided an additional optical path length of 12 m and reduced the repetition rate from 195 MHz to 11.7 MHz. Our MPC design consisted of a flat and a curved (R=4 m) high reflector, separated by 1 m. The separation distance was determined by using Eq. (2.3) for n=6 and m=2. For this particular case, the laser beam inside the MPC forms a circular spot pattern on each mirror with an angular separation of 60º between consecutive spots. Each mirror had a notch to allow the injection and extraction of the laser beam. Due to the use of notches, six full round trips are not completed by the exiting beam. To compensate for the remaining round trip and to make the MPC q-preserving, the exiting laser beam was retroreflected by using a curved mirror (R=2m, M6) positioned 1 m from the flat MPC mirror (M5).

2.4 Continuous-Wave and Femtosecond Pulse Results and Discussion

We performed continuous-wave power efficiency measurements to determine the insertion loss of the MPC. The power efficiency data are shown in Fig. 2.2. With the 2.5 % output coupler, the absorbed threshold pump power was found to increase from 290 mW to 440 mW and the slope efficiency dropped to 4.7 % after the addition of the MPC. From the increase in the pump threshold, we estimated the round-trip insertion loss of the MPC mirrors to be around 2.1 %. Since the laser light makes 24 bounces inside the MPC in one round trip, the corresponding reflection loss per bounce was less than 0.1 %. For the 4.7 %

output coupling level, the absorbed threshold pump power increased from 660 mW to 700 mW and the slope efficiency dropped to 5.5 % after the addition of the MPC.

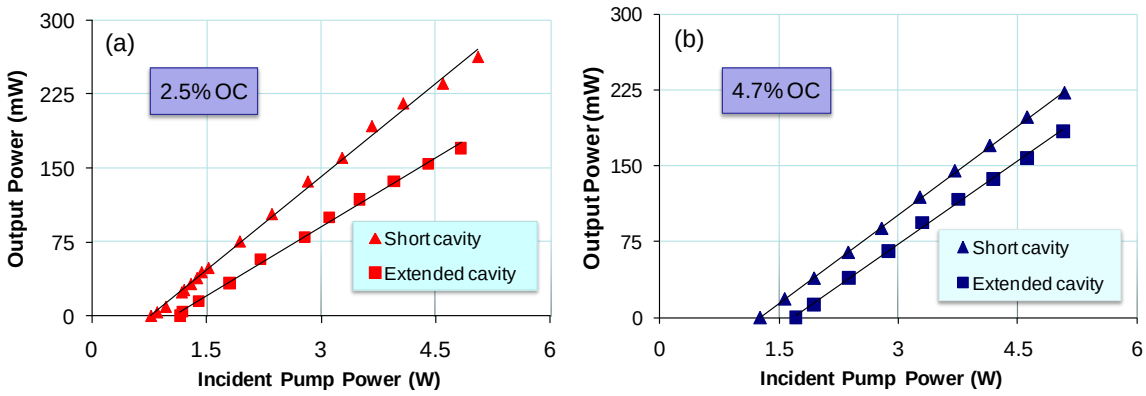

Figure 2.2: Continuous-wave power efficiency curves of the short and extended-cavity Cr^{4+}:Forsterite laser taken with (a) 2.5% and (b) 4.7 % output couplers.

After focusing inside the crystal was optimized, Kerr-lens mode-locked (KLM) operation could be readily obtained by translating the output coupler. KLM experiments were performed with both of the output couplers (4.7% and 2.5%). During the mode-locking operation, the dispersion of the cavity was controlled by using double chirped mirrors (DCMs). In the case of the 4.7% output coupler, a total of 6 DCMs (M1, M2, DCM1, DCM2, DCM3and DCM4) were included inside the cavity for dispersion compensation. The group-delay dispersion (GDD) of each DCM was about -150 fs^2, resulting in an estimated net dispersion of -1350 fs^2 per round trip, after accounting for the crystal and air dispersion. Stable KLM operation could be obtained by using 1.95 W of

absorbed pump power. In this case, the laser produced 5.1 nJ of output pulse energy with only 60 mW of average output power. Note that to obtain comparable output energies with a 100-MHz cavity would require mode-locked output powers in excess of 500 mW and pump powers approaching 10 W. Figs. 2.3(a)-(d) show the background-free autocorrelation and the spectrum of the obtained pulses by using the 4.7% and 2.5% output couplers. In the case of the 4.7% output coupler, the pulse duration was measured to be 68 fs (FWHM) by assuming a $sech^2$ pulse profile. The spectral bandwidth (FWHM) of the pulse was approximately 26 nm centered around 1278 nm, giving a time-bandwidth product of 0.33, close to the transform limit for $sech^2$ pulses. In the case of the 2.5% output coupler, 5 DCMs were used for dispersion compensation, providing a total dispersion of -1050 fs^2. Here, the laser produced 3.4-nJ pulses with a duration of 41 fs and an average output power of 40 mW. The absorbed pump power was 1.1 W. The spectral width (FWHM) of the pulses was measured to be 41 nm at 1256 nm. The time-bandwidth product was 0.32.

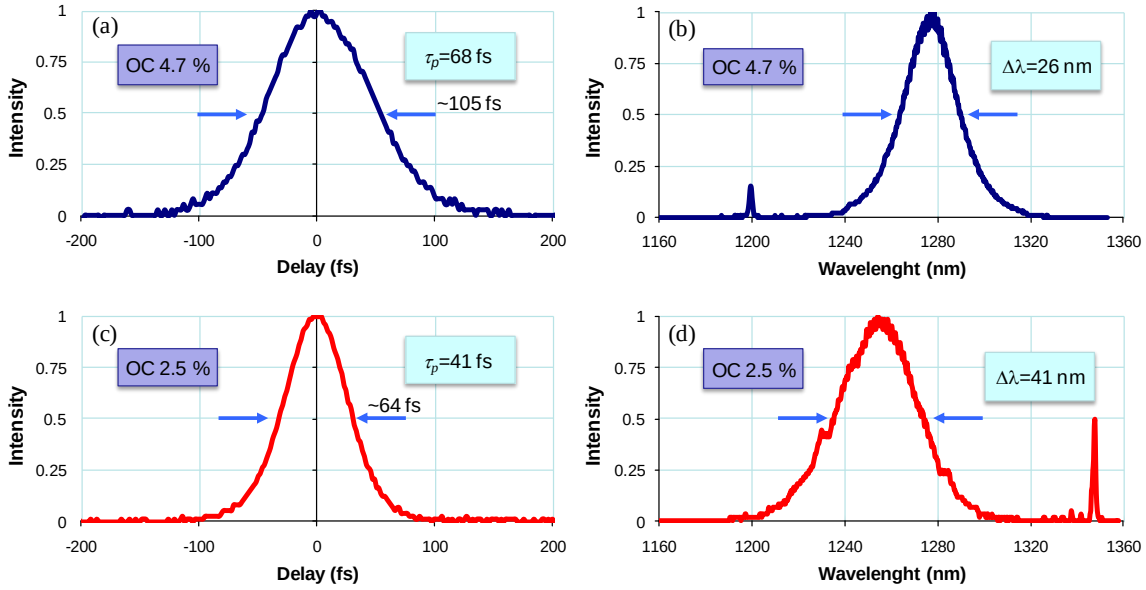

Figure 2.3: (a) Background-free autocorrelation and (b) spectrum of the pulses obtained with the 4.7 % output coupler. (c) Background-free autocorrelation and (d) spectrum of the pulses obtained with the 2.5 % output coupler. In both cases, the mode-locked MPC Cr^{4+}:Forsterite laser was operated at a pulse repetition rate of 11.7 MHz.

2.5 Summary

In conclusion, we experimentally demonstrated the mode-locked operation of a low-threshold, room-temperature, multipass-cavity femtosecond Cr^{4+}:Forsterite laser. By using a q-preserving multipass cavity, the repetition rate was lowered to 11.7 MHz. KLM operation was obtained by using two different output couplers with 2.5% and 4.7% transmission near 1260 nm. With the 4.7% output coupler, 5.1-nJ, nearly transform-limited pulses with a duration of 68 fs were generated at an output power of only 60 mW. The

absorbed pump power was 1.95 W. With a 2.5% output coupler, shorter 41-fs pulses could be obtained with a pulse energy of 3.4 nJ at an absorbed pump power of 1.1 W. We believe that femtosecond Cr^{4+}:Forsterite lasers with reduced power requirements should find widespread applications in biomedical imaging and spectroscopy.

Chapter 3

CHIRPED PULSE, MULTIPASS CAVITY Cr^{4+}:FORSTERITE LASER

3.1 Introduction:

Femtosecond laser sources with amplified pulse energies have become indispensable in many important applications such as high harmonic generation, micro machining, and multi-photon microscopy [44-45, 58]. Various techniques such as regenerative amplification or cavity dumping can be used to increase the pulse energy. However, this usually increases the cost and the complexity of the system. On the other hand, cavity extension offers a relatively simple and cost-effective method to increase the pulse energy of the mode-locked oscillator while maintaining high repetition rates in the MHz range [48, 59]. In this case, the pulse energy can be scaled up by lowering the pulse repetition rate. Furthermore, use of q-preserving multipass cavity (MPC) geometries ensures that the extended cavity remains compact and most importantly, keeps the operating point of Kerr-lens mode locking (KLM) close to that of the short cavity [48, 56]. In the high energy solitary pulse regime, a large amount of intracavity negative dispersion is also required to

balance the nonlinearities and to prevent multi-pulse instabilities as the cavity is extended. In this case, dispersion management with low loss optics becomes very challenging and expensive. Alternatively, one can resort to a chirped-pulse oscillator design, where a relatively small amount of net positive intracavity dispersion combined with KLM can also produce high-energy, picosecond pulses. The residual chirp of the output pulses can then be removed externally by using a prism or a grating pair [39-43]. Another important advantage of chirped-pulse oscillation is that the damage risk of various intracavity elements is significantly reduced due to lower pulse peak powers. In earlier studies, pulse energies as high as 0.5-μJ could be obtained from a chirped-pulse, extended-cavity Ti:sapphire oscillator [43]. Furthermore, cavity dumping could further increase the output pulse energy to 1.1 μJ [42].

In this part of the thesis, we describe on the application of the chirped-pulse oscillation technique to an extended-cavity Cr^{4+}:Forsterite oscillator operating near 1258 nm center wavelength. In the experiments, a q-preserving MPC was added to a Cr^{4+}:Forsterite laser to generate 81-nJ 5.45-ps chirped pulses with 395 mW average output power. To our knowledge, this is the highest pulse energy directly obtained from a room-temperature, mode-locked Cr^{4+}:Forsterite laser. By using an external grating pair, the pulses could be compressed down to 607 fs. The obtained results were published in the reference [60].

3.2 Experimental

A schematic and a picture of the Cr^{4+}:Forsterite oscillator and the external grating compressor setup is shown in Figure 3.1. The standard astigmatically-compensated short x-resonator, operating at a repetition frequency of 143 MHz, was extended with a q-preserving MPC. The short resonator consisted of two double-chirped curved mirrors (DCM's, M1&M2) [61] each with a radius of curvature of 100 mm, three flat high reflectors (M3, M4 and M5), and an output coupler (OC) with 4.7% transmission at 1260 nm. By using M3 and M4 to adjust the angle of inclination of the beam injected into the MPC, a circular spot pattern was obtained on the MPC mirrors. To manage the dispersion of the short cavity, a SF10 prism pair (P1&P2) was used. The high reflector and output coupler arm lengths were 50.5 cm and 43.5 cm, respectively. The 20-mm-long, Brewster-cut Cr^{4+}:Forsterite crystal, having a total absorption of 70% was positioned between M1 and M2. The crystal was wrapped in an indium foil and held inside a copper holder maintained at 20 ºC by water cooling. The Cr^{4+}:Forsterite oscillator was end-pumped with a continuous-wave (CW) Yb:fiber laser at 1064 nm. The pump beam was focused to an estimated 30-μm waist inside the crystal with a 20-cm lens (L).

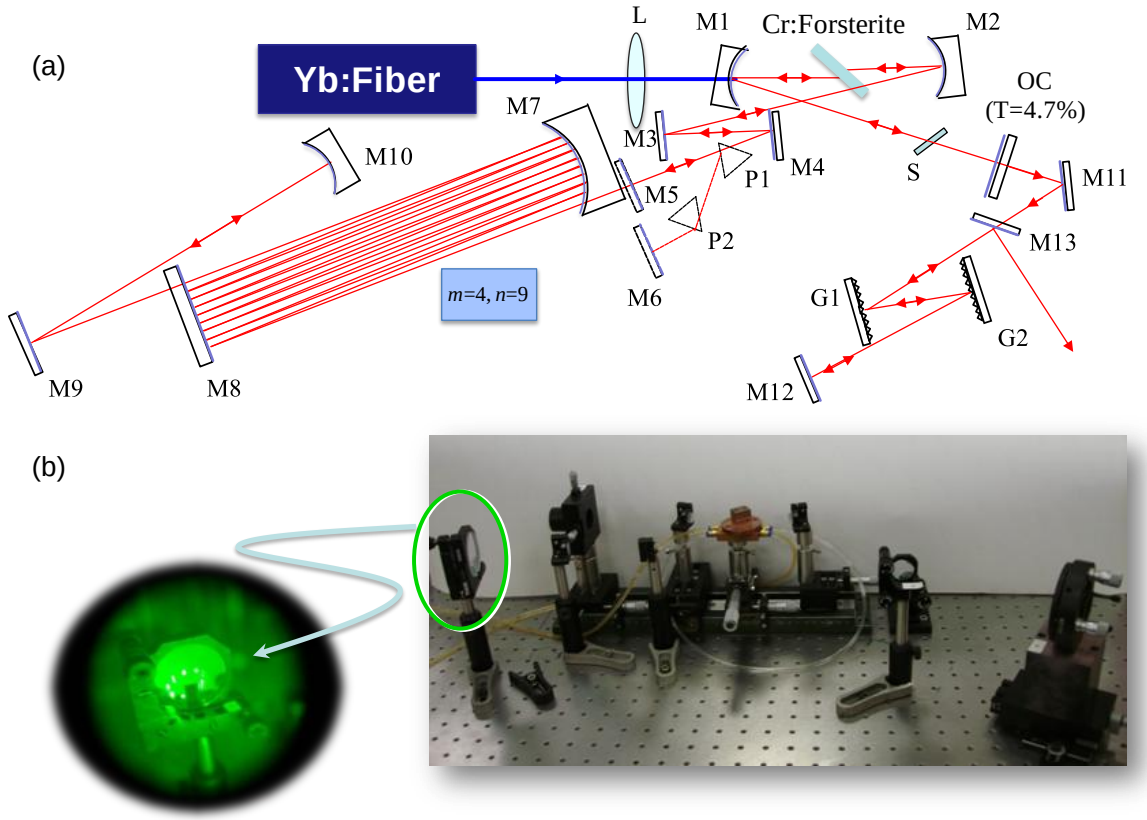

Figure 3.1: (a) Schematic and (b) picture of the multipass-cavity, chirped-pulse Cr^{4+}:Forsterite laser and the external grating compressor setup.

The cavity was extended by adding a flat-curved MPC to the high reflector arm. The flat end high reflector M5 was removed in the extended cavity. The MPC comprised a curved mirror with radius of curvature of 4 m (M7) and a flat mirror (M8), each with a notch to allow the injection and extraction of the beam. To make the MPC q-preserving, the mirror separation was set at 1.65 m and the beam exiting was retro reflected by a curved end mirror (M10, R=2 m) placed at a distance of 1.65 m from M8 [56]. The laser beam

injected into the MPC completed 9 round trips before returning back to the original cavity. The addition of the MPC provided an effective optical path length of 59.4 m, resulting in the reduction of the pulse repetition rate to 4.88 MHz. Furthermore, the extended cavity was contained within a box to minimize mode-locking instabilities due to air currents. To compress the positively chirped picosecond pulses outside the cavity, two different grating pairs (G1&G2) with groove densities of 300 grooves/mm and 600 grooves/mm were employed. The photograph of the grating compressor setup is shown in Figure 3.2.

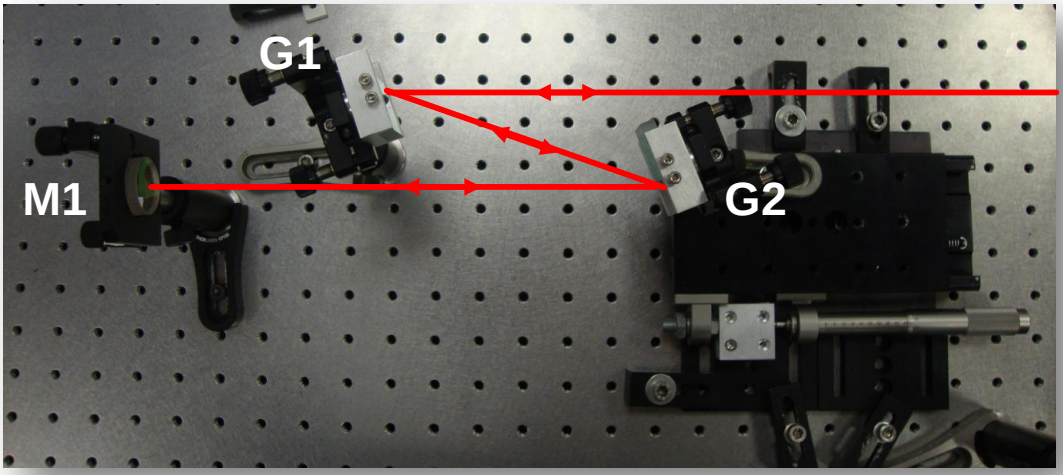

Figure 3.2: Picture of the grating compressor setup.

3.3 Continuous-Wave and Chirped-Pulse Results and Discussion

The Cr^{4+}:Forsterite laser was first operated in the CW regime. Figure 3.3 shows the CW performance of the laser with different resonator architectures. The incident threshold

pump power and the slope efficiency of the short cavity were determined to be 2.35 W and 14.6%, respectively. From the short cavity, as high as 900 mW of output power could be obtained with 8.5 W of input pump power at 21^0C. By comparing the threshold pump power at different output coupling levels, the passive loss of the short resonator was determined to be 2.9%. With the insertion of the prism pair, the slope efficiency decreased to 12.1% and the threshold pump power increased to 2.77 W. From the threshold analysis, the prism insertion loss for one-round trip was determined to be 1.13%. With the addition of the MPC to the short resonator, the threshold pump power increased to 2.65 W from 2.35 W. From the threshold analysis, the total round-trip loss of the MPC came to 0.74% corresponding to less than 0.03% loss per bounce from the MPC mirrors. The slope efficiency was further measured to be 13.3 % with respect to input pump power. As high as 740 mW output power could be obtained from the extended resonator.

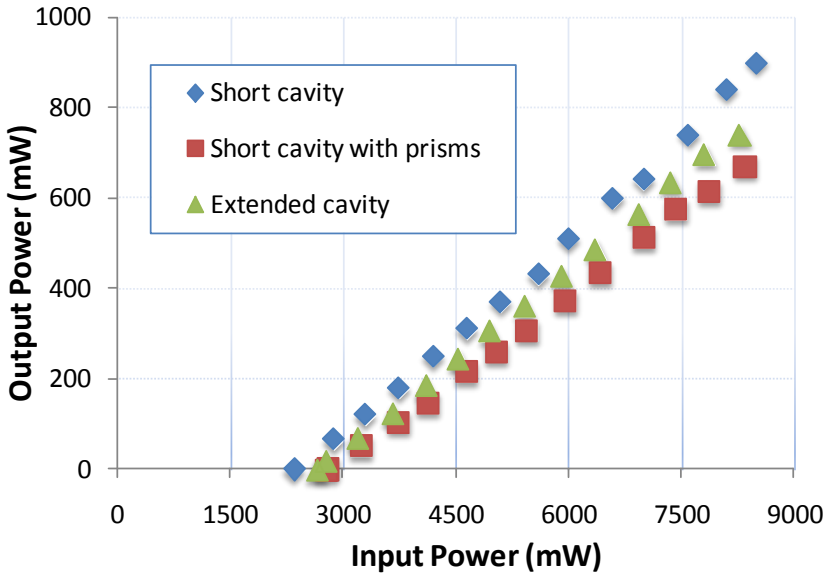

Figure 3.3: Continuous-wave power efficiency curves of the short and extended-cavity Cr^{4+}:Forsterite laser.

With the help of the SF10 prism pair whose separation was set to 15 cm, the total round-trip group delay dispersion (GDD) of the short cavity came to 300 fs^2, by taking into account the dispersion due to cavity mirrors (-600 fs^2), gain medium (800 fs^2), air path (12 fs^2), prism pair (-1147 fs^2) and prism insertion (1235 fs^2). When the focusing inside the crystal was carefully adjusted, KLM operation could be initiated by translating the output coupler. With 6.88 W of incident pump power, 2.6-nJ chirped-pulses could be produced from the short resonator. The spectral bandwidth (FWHM) of the pulses was approximately 25 nm centered around 1255 nm (see Figure 3.4). The spectrum of the pulses had a nearly

rectangular shape which is very common for chirped-pulse oscillators. The corresponding pulsewidth was measured to be 2.69 ps.

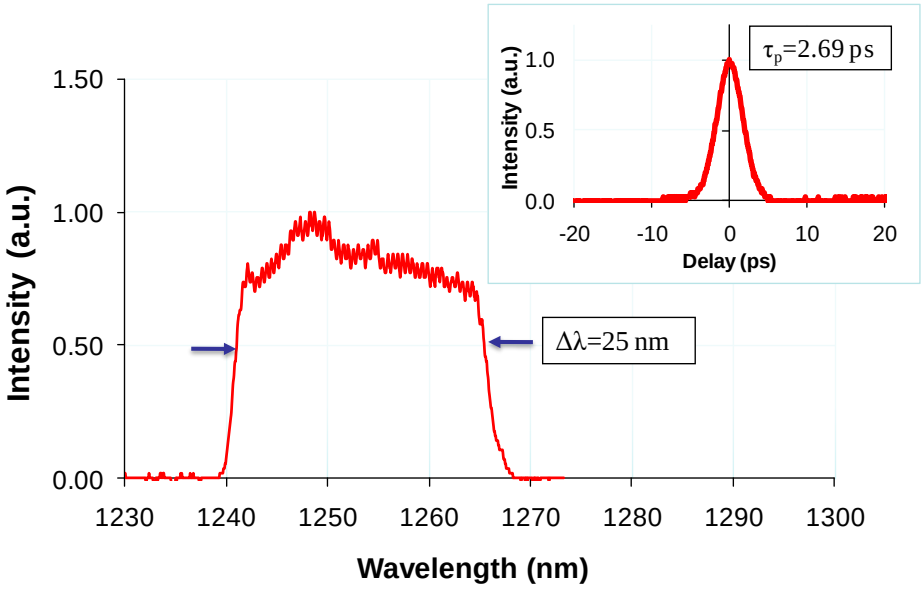

Figure 3.4: Spectrum and background-free auto-correlation of the pulses from the Kerr-lens mode-locked, chirped-pulse short-cavity Cr^{4+}:Forsterite laser.

During mode-locked operation of the extended-cavity Cr^{4+}:Forsterite laser, a 1-mm SF11 glass slab was added to the cavity to control the dispersion level. The corresponding total GDD of the cavity was estimated to be 1480 fs^2 by also accounting for the dispersion due to MPC mirrors (approximately 10 fs^2 per bounce). In this case, the laser generated as high as 81-nJ pulses with an average output power of 395 mW at the input pump power of 8 W. To our knowledge, this is the highest pulse energy obtained directly from a room-temperature, mode-locked Cr^{4+}:Forsterite laser. Figures 3.5 show the spectrum and

background-free auto-correlation signal of the pulses, respectively. The spectral bandwidth (FWHM) was approximately 21 nm centered around 1258 nm and the corresponding pulse width (FWHM) was 5.45 ps in the chirped pulse oscillation regime. Once initiated, stable mode-locked operation could be sustained for up to nearly 30 minutes. Total GDD levels larger than 1480 fs^2 reduced the spectral bandwidth of the chirped pulse oscillator. No multi pulsing was observed in the picosecond and nanosecond time scales. The ripples in the spectrum were due to back reflections in the uncoated beamsplitter used to do simultaneous spectrum and autocorrelation measurements. The critical intracavity laser power for self focusing and the corresponding total nonlinear phase shift inside the gain medium were estimated to be 2.4 MW and 4.3, respectively [62] by using the nonlinear refractive index value of 6 $x10^{-16}$ cm^2/W for Cr^{4+}:Forsterite [63]. At the highest output energy of our oscillator (intracavity peak power=287 kW), the nonlinear phase shift was determined to be around 0.5. This suggests that self-focusing was not limiting the pulse energy in the experiments and a further, 8-fold increase in output energy appears possible.

The pulses were then compressed outside the cavity by using grating pairs (G1 and G2). We tested two grating pairs with 300 grooves/mm and 600 grooves/mm. The gratings were positioned close to double-pass Littrow configuration. The grating separation distance was varied to obtain the shortest pulses.

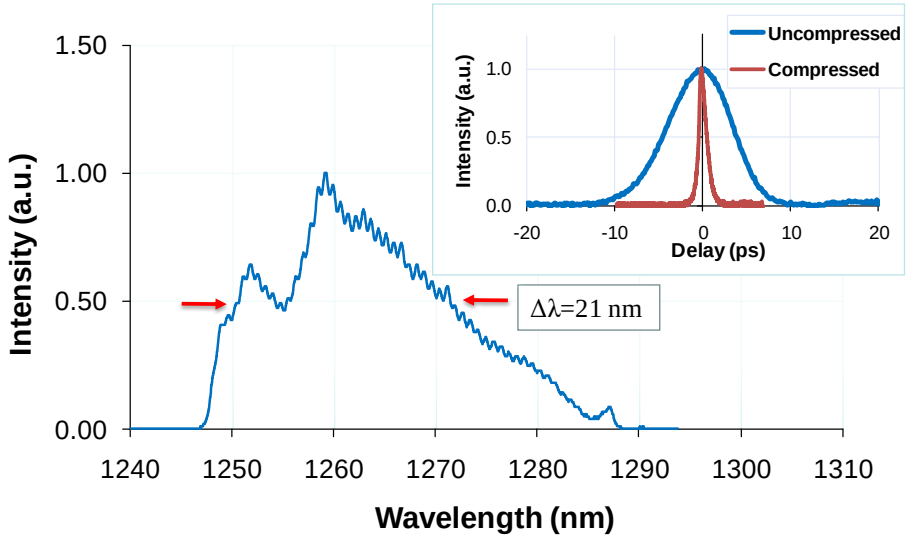

Figure 3.5: Spectrum and background-free auto-correlation of the original (uncompressed) and compressed pulses from the Kerr-lens mode-locked, chirped-pulse MPC Cr^{4+}:Forsterite laser.

Figure 3.6 shows the variation of pulse duration as a function of grating spacing for the grating pair with 300 grooves/mm. As can be seen, the pulses could be compressed to as short as 607 fs when the grating separation was adjusted to 52 cm. For the particular separation and angle of incidence used, the corresponding GDD and the third-order dispersion were estimated to be -330.000 fs^2 and $7.1x10^5$ fs^3, respectively. Figure 3.5 also shows the background-free auto-correlation signal of the chirped and compressed pulses. At the exit of the compressor, the pulse energy was measured to be 28.4 nJ corresponding to a peak power of 46.7 kW. From the pulse energies at the entrance and exit of the compressor setup, the compressor throughput was measured to be 35%. For the grating pair with 600 grooves/mm, the pulses could be compressed to a slightly larger pulse duration of

620 fs. The corresponding grating separation was 12.1 cm, providing a GDD close to the value for the other grating pair. However, the estimated third-order dispersion ($9.3x10^5$ fs^3) for this grating pair was considerably larger. As a result, we can attribute the minimum pulse duration being longer than the Fourier-transform limit to the presence of higher order spectral phase distortions. At the exit of the compressor, the pulse energy was 37 nJ, giving a peak power of 60 kW. The overall efficiency of the compressor setup in this case was 46%. We believe that use of gratings with higher diffraction efficiency should increase the available pulse energy after compression.

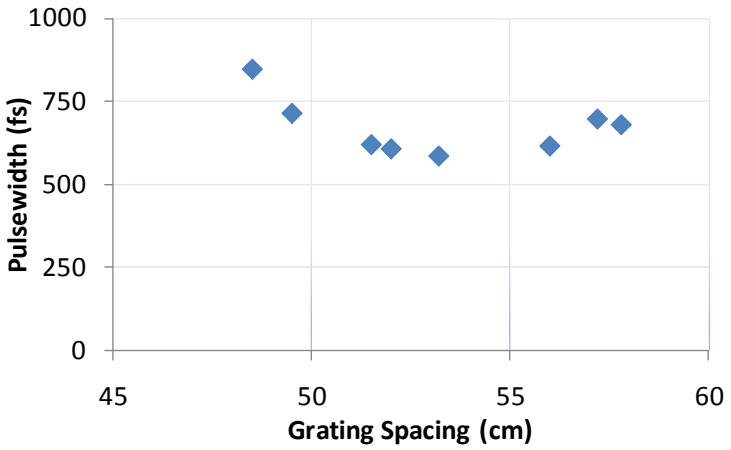

Figure 3.6: Pulse duration of the compressed pulses as a function of the grating separation distance for the grating pair having grove density of 300 grooves/mm.

3.4 Summary

In conclusion, we have obtained record 81-nJ pulses directly from a room-temperature, chirped-pulse, multipass-cavity Cr^{4+}:Forsterite oscillator operating at 4.9 MHz. External

compression with a grating pair resulted in 607-fs pulses at the wavelength of 1258 nm. High-energy mode-locked oscillators operating in this wavelength range should be important in various biomedical applications including deep-tissue multi-photon microscopy as well optical coherence tomography.

Chapter 4

Nd^{3+}:TELLURITE GLASS LASER

4.1 Laser Operation at 1065 nm

4.1.1 Introduction

There has been a great deal of interest in the development of efficient laser glasses due to the ease and low cost of their preparation. Among possible candidates, tellurite-based glasses are particularly attractive because of numerous favorable physical characteristics, including a wide transparency range (0.35-5.0 μm), lower phonon energy (700-750 cm^{-1}) than other widely used glass hosts such as borates or silicates, high linear and nonlinear refractive index, good chemical stability, and resistance to moisture [64]. In earlier studies, our group performed detailed spectroscopic investigation and Judd-Ofelt analysis of various thulium-doped tellurite glasses [65-66]. Recently, lasing has been reported in Nd^{3+}-doped TeO_2–TiO_2–Nb_2O_5 glasses [67]. In this case, lasing at 1064 nm was confirmed by analyzing the time-dependent emission profiles at 1064 nm.

In this part of the thesis, lasing in a novel, neodymium-doped tellurite-based glass (Nd:Tellurite) with the host composition $(0.8)TeO_2$-$(0.2)WO_3$ will be described. To our best knowledge, this is the first time laser operation from Nd:Tellurite glass with this composition reported in the literature [23]. Neodymium ions were introduced by adding 0.5 mol. % Nd_2O_3 into the glass. The doped sample was placed inside a four-mirror cavity and end-pumped by a pulsed Ti^{3+}:Al_2O_3 laser at 805 nm. During gain switched operation, the glass laser produced 11 μJ of output energy at 1065 nm with 114 μJ of pump. The slope efficiency with respect to incident energy was 12%. These results indicate that doped tellurite glasses have the potential of being used in the development of efficient bulk glass lasers and fiber lasers.

4.1.2 Experimental

The glass sample was prepared by heating a powder mixture of Nd_2O_3 (99.9% purity), TeO_2 (99.999% purity) and WO_3 (99% purity) inside an air-filled furnace at 800 ºC for 1 hour. After quenching the melt in air at room temperature, it was annealed at 250 ºC for 1 hour. Composition of the mixture was 0.5 mole of Nd_2O_3 for every 100 moles of $(0.8)TeO_2$-$(0.2)WO_3$. The Nd^{3+} ion concentration for the 4.1-mm long sample was determined to be 2.05×10^{20} cm^{-3}. The small-signal single-pass absorption at the pump wavelength of 805 nm was measured to be 0.92, corresponding to an absorption coefficient of 6.04 cm^{-1}. In order to measure the time-dependent fluorescence, the sample was excited

at 805 nm with a pulsed Ti^{3+}:Al_2O_3 laser which produced 60-ns pulses at a pulse repetition rate of 1 kHz. The fluorescence lifetime of the sample was determined to be 142 μs .

A schematic of the laser setup is shown in Figure 4.1. The Nd:Tellurite sample was placed inside an astigmatically compensated x-cavity consisting of two curved mirrors (M1 and M2, R=10 cm), a flat highly reflecting end mirror (M3), and a flat output coupler (OC) with a transmission of 3.3 %. Lasing was also obtained by replacing the output coupler with a high reflector to estimate the passive resonator losses. The high reflector and the output coupler arms were 100 cm and 54 cm, respectively. From the standard ABCD analysis of the cavity, the laser beam waist was estimated to be 21 μm. The resonator was end pumped by a pulsed Ti^{3+}:Al_2O_3 laser (repetition rate=1 kHz) at 805 nm. An input lens (L) with a focal length of 10 cm was used to focus the pump beam inside the glass sample. The pump beam waist was measured by using the knife-edge technique to be 29 μm.

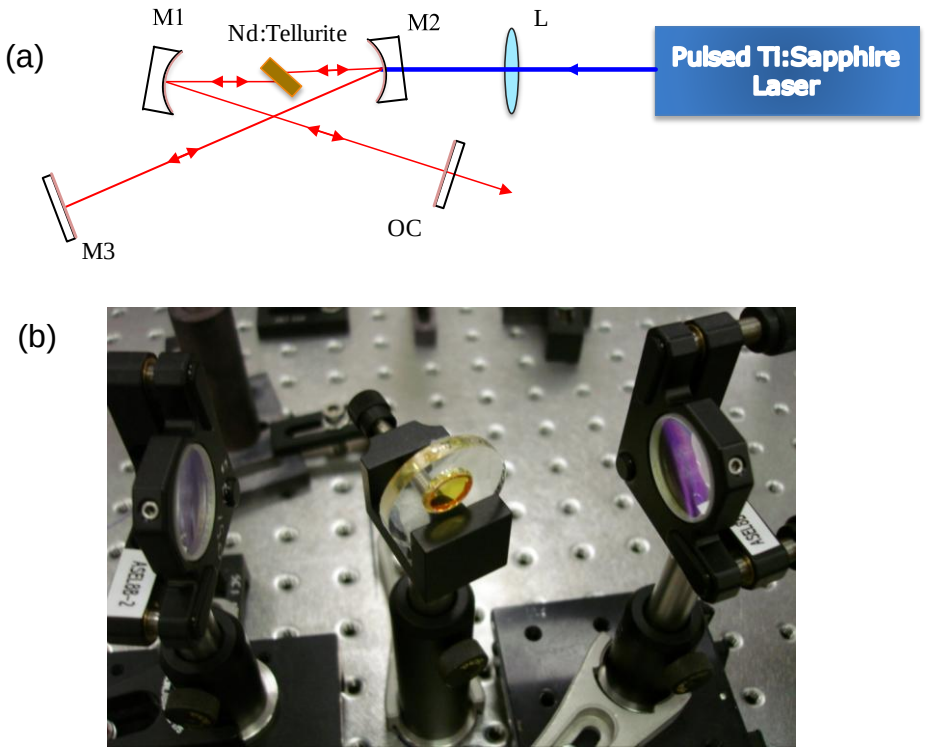

Figure 4.1: (a) Schematic of the gain-switched Nd:tellurite laser (b) picture of the glass sample.

4.1.3 1065 nm Glass Laser Results and Discussion

After optimizing the cavity alignment, gain switched lasing was obtained at 1065 nm. Figure 4.2 shows the results of the energy efficiency measurements. Lasing was obtained at an incident threshold pump energy of 19 μJ by using the 3.3% output coupler. The slope efficiency was 12%. When a high reflector was used as the output coupler, the incident threshold pump energy was reduced to 13 μJ. By assuming that the threshold pump energy is directly proportional to (L+T) (L=roundtrip cavity loss, T=output coupler transmission), the round trip loss was determined to be 8.1%. The output pulse profile varied with pump

energy. At the incident pump energy of 114 μJ, the pump and the laser pulsewidths (FWHM) were measured to be 60 ns and 270 ns, respectively.

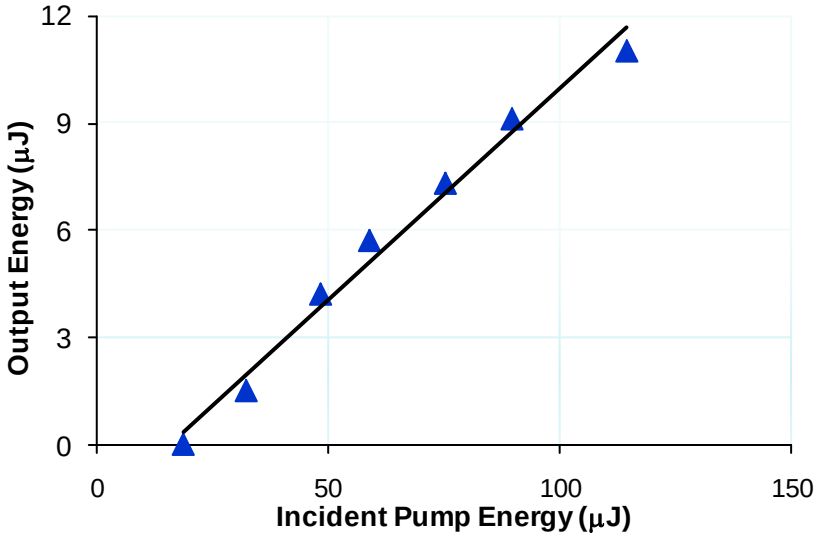

Figure 4.2: Energy efficiency curve for the 0.5 mol% Nd_2O_3:(0.8)TeO_2-(0.2)WO_3 glass laser.

We estimated the emission cross section σ_L of the Nd:Tellurite glass from the threshold data. In the limit where the pump pulsewidth is much shorter than the fluorescence lifetime, which was the case in our experiment, the incident threshold pump energy E_{th} is given by [68]

$$E_{th} = \frac{\pi h\nu_p (w_L^2 + w_p^2)(T + L_r)}{4\eta_a \sigma_L}, \tag{4.1}$$

where $h\nu_p$ is the pump photon energy, w_L is the laser spotsize, w_P is the pump spot size, and η_a is the absorption at the pump wavelength. Using E_{th}= 13 μJ, w_L=21 μm, w_P=29 μm, T=0 (for the high reflector), L_r =0.081, η_a=0.92, the emission cross section σ_L for the 0.5 mol.% Nd_2O_3:(0.8)TeO_2-(0.2)WO_3 glass sample was determined to be 1.64 x 10^{-20} cm^2 at 1065 nm.

4.1.4 Summary

In conclusion, we reported on the first observation of lasing in bulk, Nd^{3+}-doped (0.8)TeO_2-(0.2)WO_3 glass at 1065 nm. The results indicate the potential of this tellurite-based glass in the development of bulk glass or fiber lasers.

4.2 Laser Operation at 1370 nm

4.2.1 Introduction

There is a growing demand for coherent light sources operating in the 1.3-1.4 μm window for biomedical imaging applications [44, 69]. In comparison with more widely used sources at 800 nm and 1 μm, use of higher wavelength lasers significantly decreases the losses due to Rayleigh scattering and enables deeper tissue penetration. Furthermore, staying below 1.4 μm avoids water absorption losses. As potential laser hosts, glasses offer several advantages over single crystals, including far lower cost, simpler preparation techniques, and the possibility of power scaling when drawn into fiber. Due to these advantages, there have been many studies aimed at the development of glass lasers doped with rare-earth ions. In the particular case of neodymium (Nd^{3+})-doped systems, lasing has been reported in various glass matrices including fluorides [70-71], chalcogenides [72], aluminosilicates [73], germinates [74], and tellurites [23, 67, 75-76]. Among these, tellurite-based glasses have attractive properties including wide transparency range (0.35-5.0 μm), high refractive index, lower non-radiative decay rates than silicates, phosphates or germanates, and resistance to corrosion [64, 77-78]. In addition, tellurite-based glasses are considered to be strong candidates as laser host materials because they have the highest emission cross-section among the Nd^{3+}-doped oxide glasses [77]. To date, lasing could be obtained from a bulk tellurite glass from the $^4F_{3/2} \rightarrow {}^4I_{11/2}$ transition of Nd^{3+} ion [23, 67, 75-76] which corresponds to the wavelength of around 1064 nm. However lasing operation

has not been achieved so far for the $^4F_{3/2} \rightarrow {}^4I_{13/2}$ transition which generates radiation in the 1.34-1.37 μm spectral region.

In this part of the thesis, we report for the first time to our knowledge, lasing action at 1370 nm from $^4F_{3/2} \rightarrow {}^4I_{13/2}$ transition of Nd^{3+} ion in a bulk tellurite glass host where the emission cross section is lower than that for the $^4F_{3/2} \rightarrow {}^4I_{13/2}$ transition. The obtained results were published in the reference [22]. The glass sample had a composition of $(0.8)TeO_2$-$(0.2)WO_3$ with 0.5 mol. % Nd_2O_3. The laser could be operated in gain-switched regime at 1 kHz with as low as 59 μJ of threshold pulse energy. In addition, the slope efficiency was determined to be 5.5 %. As a pump source, we used a pulsed Ti.Sapphire laser at the wavelength of 805 nm. From the analysis of threshold data, we determined the emission cross section to be 1.57 x 10^{-20} cm^2 at the wavelength of 1370 nm. Lasing could not be obtained over the broad emission band, believed to be due to excited-state absorption. By using the lasing efficiency data, we further estimated the excited state absorption cross section σ_{ESA} to be 1.22 x 10^{-20} cm^2. The ratio of the excited state and stimulated emission cross sections (0.78) is consistent with the reported value obtained for SiO_2- based Nd:glass fiber operating at 1.36 μm [79].

4.2.2 Experimental

The tellurite glass sample was prepared with the composition of Nd^{3+}:$(0.8)TeO_2$-$(0.2)WO_3$ by melting the powder mixtures of Nd_2O_3 (99.9% purity), TeO_2 (99.999% purity), and

WO_3 (99% purity). The batch containing 0.5 mole of Nd_2O_3 to 100 moles of $(0.8)TeO_2$-$(0.2)WO_3$ was mixed and melted in a platinum crucible at 800 ºC for 1 hour in an electrically heated furnace in ambient air atmosphere. Then, the glass melt was rapidly quenched in a preheated stainless steal mold at the temperature around 150 ºC. To release the residual thermal stresses formed in the glass during the quenching process, the sample was annealed below the glass transition temperature at 250 ºC. Sample surfaces were then polished to a thickness of 4.1 mm. Using the measured density of 5.82 gm/cm^3, the Nd^{3+} ion concentration was determined to be 2.02×10^{20} cm^{-3}. The single-pass absorption at the pump wavelength of 805 nm was 92 %.

Figure 4.3 shows a schematic and the picture of the standard astigmatically compensated x-cavity laser setup. The cavity consisted of two curved highly reflecting mirrors with radius of curvature 5 cm (M1 and M2), a flat end high reflector (M3), and a flat output coupler with transmission of 2.5 % at 1370 nm (OC). The highly reflecting mirrors have reflectivity above 99.9 % in the range of 1150-1450 nm and transitivity above 90 % at 1065 nm which prevents laser operation at that wavelength. As a pump source, we used a home-made, tunable, pulsed Ti:sapphire laser at 805 nm with a pulse repetition rate of 1 kHz. The output of the pump laser was focused inside the glass sample by using a lens with a focal length of 5 cm. The pump beam waist was measured to be 27 μm with the knife-edge technique. The high reflector and output coupler arm lengths were 31 and 32 cm, respectively, giving an estimated beam waist of 21 μm near the middle of the stability

range. The time dependent fluorescence signal and pulse traces of glass and pump lasers were measured with a digital oscilloscope and a Ge PIN detector (response time of 3.5 ns). Emission spectrum and wavelength measurements were performed with a ½-m Czerny-Turner-type monochoromator and a PbS detector coupled with a lock-in amplifier.

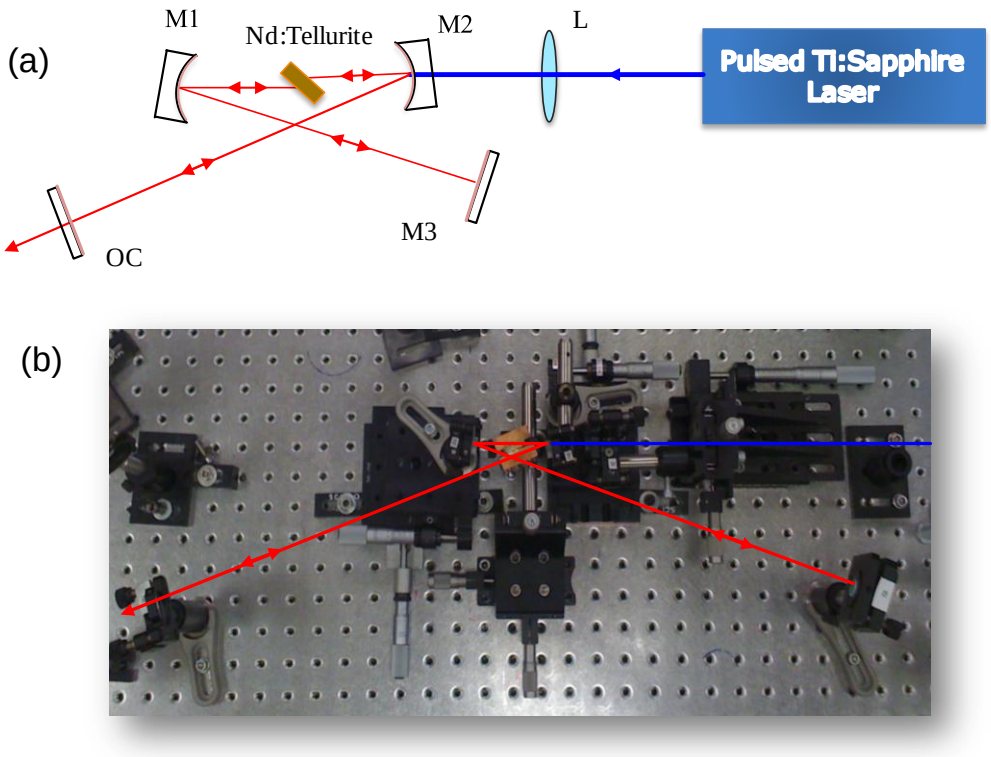

Figure 4.3: (a) Schematic and (b) picture of the gain-switched, bulk neodymium-doped tellurite (Nd^{3+}:TeO_2-WO_3) glass laser.

4.2.3 1370 nm Glass Laser Results and Discussion

The power efficiency curve of the Nd^{3+}:Tellurite glass laser operating at 1370 nm is shown in Figure 4.4. The slope efficiency of the laser was determined to be 5.5 % with respect to the incident pump pulse energy. The laser could be operated with as low as 59 μJ of incident threshold pulse energy and we obtained as high as 6 μJ of output pulse energy. To determine the passive loss of the resonator, the threshold pump power of the laser was also measured by replacing the output coupler with a flat high reflecting mirror. The corresponding threshold energy decreased to 32 μJ. By comparing the threshold pulse energy for two different output coupling levels, we determined the round trip passive loss of the cavity (L_r) to be 2.9 %. Here, we assumed that the threshold pump energy is directly proportional to ($L_r + T$) where T is the output coupling level. Furthermore, the optimum output coupling level can be found by using the formula, $T_{opt} = L_r\left(\sqrt{r} - 1\right)$, where r is the ratio of maximum available pump pulse energy to the threshold pulse energy ($r = E_p / E_{th}$) for zero output coupling (32 μJ). In our case, the optimum output coupler level came to be about 3.8 % at the maximum available pump energy of 169-μJ. The corresponding estimated output energy for optimum output coupling becomes 6.5 μJ which is close to experimentally obtained pulse energy with the 2.5 % output coupler.

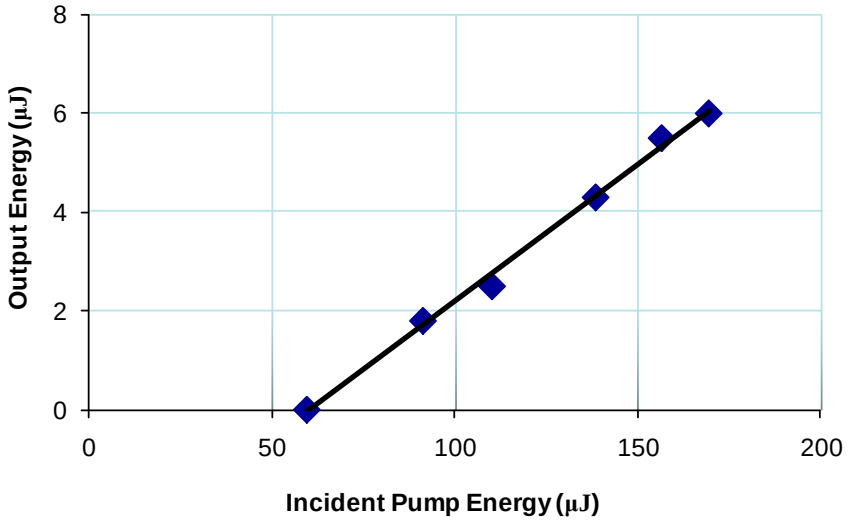

Figure 4.4: Energy efficiency curve of Nd^{3+}:Tellurite glass laser. The slope efficiency is around 5.5 %. The transmission of the output coupler (OC) is 2.5 % at 1370 nm.

Figure 4.5 shows the time-dependent fluorescence decay curve for the $^4F_{3/2} \rightarrow {}^4I_{13/2}$ transition. From the decay data, the fluorescence lifetime was determined to be 114 μs. In our previous study about 1065 nm laser action of the same host, the fluorescence lifetime for the $^4F_{3/2} \rightarrow {}^4I_{11/2}$ transition was measured to be 142 μs [23] which is close to what we had for the $^4F_{3/2} \rightarrow {}^4I_{13/2}$ transition, as expected.

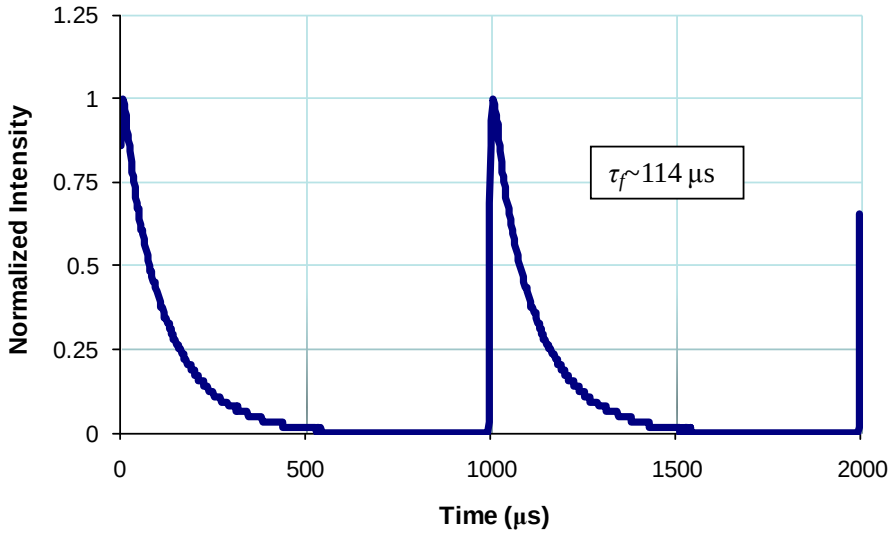

Figure 4.5: Fluorescence decay curves for the Nd^{3+}:Tellurite glass sample at 1.37 µm. The fluorescence lifetime is around 114 µs.

Furthermore, Figure 4.6 shows the temporal profile of the output laser pulses at different pump energies. As can be seen, the output pulse width drops from 3.37 to 1.74 µs as the pump pulse energy increases from 110 to 170 µJ. In this pumping level range, the pump pulse width remains almost constant around 116 ns. In Figure 4.6, the lower peaks preceding the laser pulses were the pump laser pulses which could not be completely eliminated by the filter. The delay between the pump and laser pulses depended on the pumping level as expected and decreased from 7.4 to 5.6 µs as the incident pump energy was increased from 110 to 170 µJ.

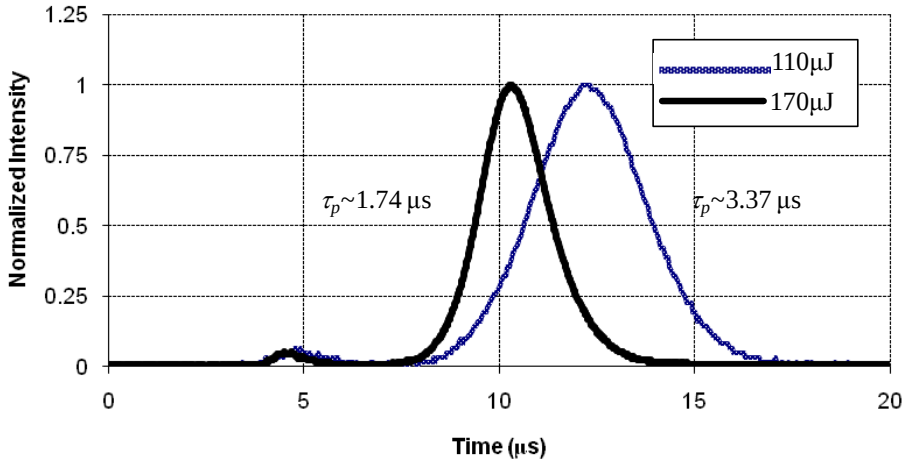

Figure 4.6: Temporal profiles of the laser pulses at a pump energy of 110 μJ and 170 μJ.

Figure 4.7 shows the emission spectrum of the glass sample and laser emission. As can be seen from the spectrum, there are two peaks around 1065 and 1342 nm which correspond to the transitions $^4F_{3/2} \rightarrow {}^4I_{11/2}$ and $^4F_{3/2} \rightarrow {}^4I_{13/2}$, respectively. From the spectrum measurements, one would expect to get lasing at the peak wavelength of 1342 nm. However, previous studies show that there is a competing excited-state absorption (ESA) at the peak emission wavelength [79-81]. As can be seen from the energy level diagram of Nd^{3+} ion (Figure 4.8), there are two excited state absorption transitions $^4F_{3/2} \rightarrow {}^2G_{9/2}$ and $^4F_{3/2} \rightarrow {}^4G_{7/2}$ which correspond to the wavelengths around 1 μm and 1.34 μm, respectively. The transition $^4F_{3/2} \rightarrow {}^2G_{9/2}$ does not introduce any significant loss at 1065 nm laser operation even though it is close to the lasing wavelength [71]. However, ESA due to

$^4F_{3/2} \rightarrow {}^4G_{7/2}$ transition introduces extra loss near the peak of the 1342-nm emission and shifts the laser wavelength to 1.37 μm. To check whether the ambient humidity has any effect on the emission wavelength, we further purged the whole resonator with pure N_2 gas and lowered the relative humidity level from 50 to 12 %. No observable change was recorded in the lasing wavelength or the output power of the laser.

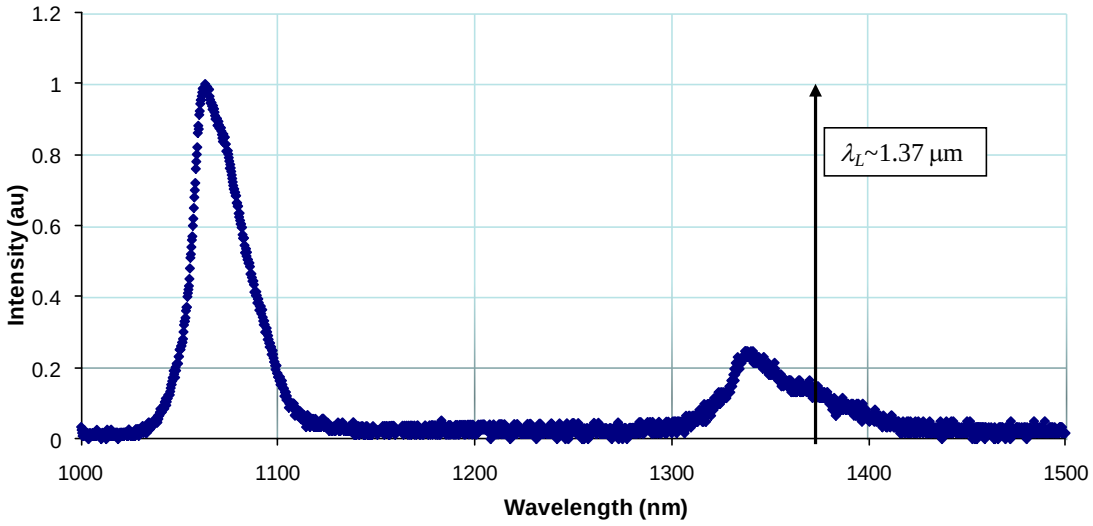

Figure 4.7: Emission spectrum of the Nd^{3+}:Tellurite glass sample in the 1000-1500 nm range. The laser was operating at 1.37 μm.

The slope efficiency of the laser was used to estimate the ratio of ESA cross section (σ_{ESA}) to the emission cross section (σ_L), ($f_L=\sigma_{ESA}/\sigma_L$). By assuming that the pump and laser beams are nearly matched inside the gain medium, f_L can be estimated from [82],

$$\eta = \frac{T}{(T + L_r)} \frac{\lambda_p}{\lambda_L} \eta_a (1 - f_L). \tag{4.2}$$

Here, η is the slope efficiency of the laser, η_a is the absorption at the pump wavelength, and λ_p and λ_L are the wavelengths of the pump and the laser beams, respectively. For our case, we estimated f_L to be 0.78 which is in very good agreement with the reported value for Nd:SiO_2 glass fiber operating at 1.36 μm (0.78) [79]. In addition, we determined the emission cross section (σ_L) at 1.37 μm from the threshold pulse energy value by taking ESA into account. Under the approximation that the pump pulse width is shorter than the fluorescence lifetime, the emission cross section can be determined by using the formula [82],

$$\sigma_L = \frac{\pi h \nu_p (w_L^2 + w_p^2)(T + L_r)}{4\eta_a E_{th}(1 - f_L)}, \tag{4.3}$$

where E_{th} is the threshold pulse energy, υ_p is pump photon frequency, h is the Planck constant, w_L and w_p are the laser and pump spotsizes inside the gain medium, respectively. Since the spotsize function varies within the gain medium due to diffractive spreading, we approximated w_L and w_p in Eq. (4.3) by their root-mean-squared (rms) values which came to w_L=24μm and w_p=35μm , respectively. If $w(z)$ is the spotsize function of one of the beams, the corresponding rms value w_{rms} is calculated by using

$$w_{rms} = \sqrt{\frac{1}{L_0}\int_0^{L_0} w^2(z)dz} \ . \tag{4.4}$$

Here L_0 is the length of the glass. With E_{th}= 32 μJ, T=0 (for the high reflector), L =0.029, η_a=0.92, the emission cross section, σ_L, was determined to be 1.57 x 10^{-20} cm^2 at 1.37 μm.

Moreover, by using the calculated f_L value, the excited state absorption cross section was estimated to be 1.22 x 10^{-20} cm^2 at the wavelength of 1.37 μm.

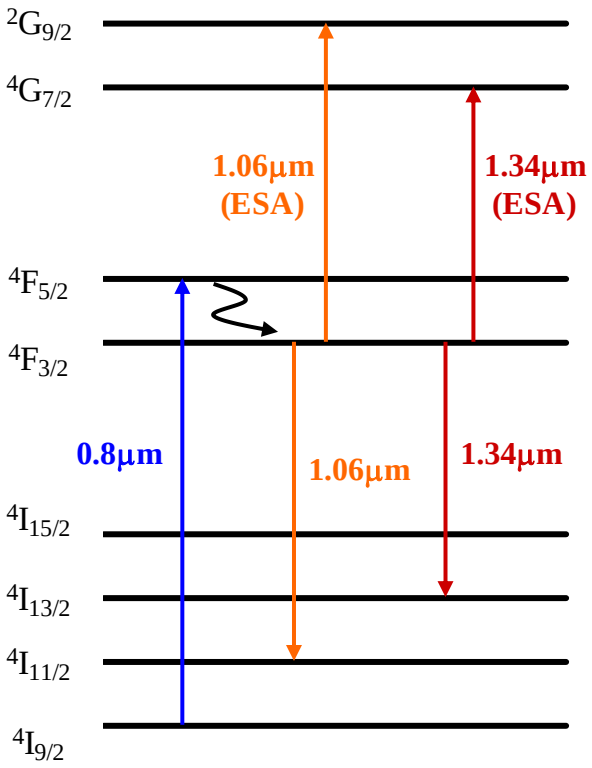

Figure 4.8: Schematic of the partial energy level diagram for the Nd^{3+} ion, showing the laser and excited state absorption transitions.

4.2.4 Summary

In conclusion, we have reported for the first time to our knowledge, lasing action at 1370 nm in a bulk tellurite glass from the energy transition $^4F_{3/2} \rightarrow {}^4I_{13/2}$ of the Nd^{3+} ion. The laser was operated in gain-switched regime at 1 kHz with a threshold pulse energy of 59

μJ. The slope efficiency was further determined to be 5.5 %. As high as 6μJ-pulses with duration of 1.74 μs were obtained. From the threshold analysis, the emission cross section came to 1.57 x 10^{-20} cm^2 in the presence of excited-state absorption. In addition, the excited-state absorption cross section, σ_{ESA} was estimated to be 1.22 x 10^{-20} cm^2 by using the slope efficiency analysis. The ratio of excited state to stimulated emission cross section is consistent with the reported value in the literature [79]. The performance of the Nd^{3+} doped tellurite glass laser was limited by excited state absorption. However, the tellurite glass host is still promising when doped with other ions such as Pr^{3+} which has optical transitions in the same spectral region and is less susceptible to excited state absorption. Hence, it should be possible to develop efficient near infrared laser systems based on tellurite glass host.

Chapter 5

EFFICIENT INJECTION-SEEDED, GAIN-SWITCHED TUNABLE Cr:ZnSe LASER

5.1 Introduction:

Cr:ZnSe lasers with broad tunability in the 2-3 μm range find a multitude of applications in the pumping of optical parametric oscillators in the mid infrared [83], generation of frequency combs for vibrational spectroscopy of molecules [84], and remote sensing [30]. All of these applications require a coherent light source which has a well defined spectral output and which is tunable. Due to the high stimulated emission cross section, 4-level energy structure, and absence of excited-state absorption in Cr:ZnSe, it is quite straightforward to obtain efficient lasing with low threshold [85-89]. However, especially during gain-switched operation where the gain far exceeds the losses, this also leads to simultaneous lasing over a very broad spectral bandwidth (of the order of tens of nanometers, often exceeding 100 nm) and limits the effective use of the laser in the applications mentioned above. One approach to remedy this problem is via use of intracavity wavelength selective elements such as diffraction gratings [32, 90]. However,

the additional insertion loss introduced by the diffraction grating increases the lasing threshold and limits the available output powers from the oscillator. An alternative approach employs injection seeding whereby the spectral characteristics of the gain-switched laser is controlled by the seed laser having a narrower spectrum. Since the seed laser is coupled into the oscillator via an end mirror, no intracavity wavelength selective elements are needed and no additional losses are introduced. Furthermore, if the seed source is tunable, it is possible to tune the output wavelength of the oscillator over the available bandwidth of the gain medium.

In this part of the thesis, we describe an injection-seeded, gain-switched Cr:ZnSe laser with considerably improved spectral brightness. After employing injection seeding, the output linewidth (FWHM) of the oscillator was reduced from 125 nm to 0.65 nm. As the seed light source, we used a second tunable continuous-wave (CW) Cr:ZnSe laser. By tuning the seed Cr:ZnSe laser with an intracavity prism, the output wavelength of the injection-seeded laser could be varied from 2255 to 2455 nm. The gain-switched laser produced as high as 157 μJ of output energy at the wavelength of 2395 nm with 598 μJ of incident pump energy (pump wavelength of 1570 nm) at a repetition rate of 1 kHz. The results were submitted to Optics Letters journal during the preparation of the thesis [91].

5.2 Experimental

Figure 5.1 shows the experimental setup of the injection-seeded gain-switched Cr:ZnSe laser. As the seed laser, we used a CW tunable Cr:ZnSe laser pumped by a Tm:fiber laser. The resonator of the CW seed laser consisted of two curved mirrors, each with a radius of curvature of 10 cm (M1 and M2), a flat end high reflector (M3) and a flat 3 % transmitting output coupler (OC1). A 2.5-mm-long Cr:ZnSe crystal (C1) was positioned between M1 and M2 at Brewster incidence. The crystal had a small-signal absorption of 94 % at the pump wavelength of 1800 nm. The crystal was surrounded with indium foil and clamped between two copper holders whose temperature was kept at 21^0C by water cooling. The pump beam was focused inside the crystal with a convex lens (L1, focal length=7.5 cm). In the high reflector arm of the resonator, a Brewster cut CaF_2 prim (P) was placed to tune the output. An adjustable slit (S) was positioned between the prism and the end high reflector to reduce the spectral width of the seed laser. The output of the CW seed laser was collimated with a curved mirror (M4, radius of curvature= 2 m) and passed through a Faraday isolator to protect the CW Cr:ZnSe laser from back reflections as well as from pulses originating from the gain-switched laser. The Faraday isolator consisted of two thin-film polarizers (TFP1 and TFP2), and halfwave plate (HWP1), a Faraday rotator (FR) and a flat aluminum retroreflecting mirror (M5).

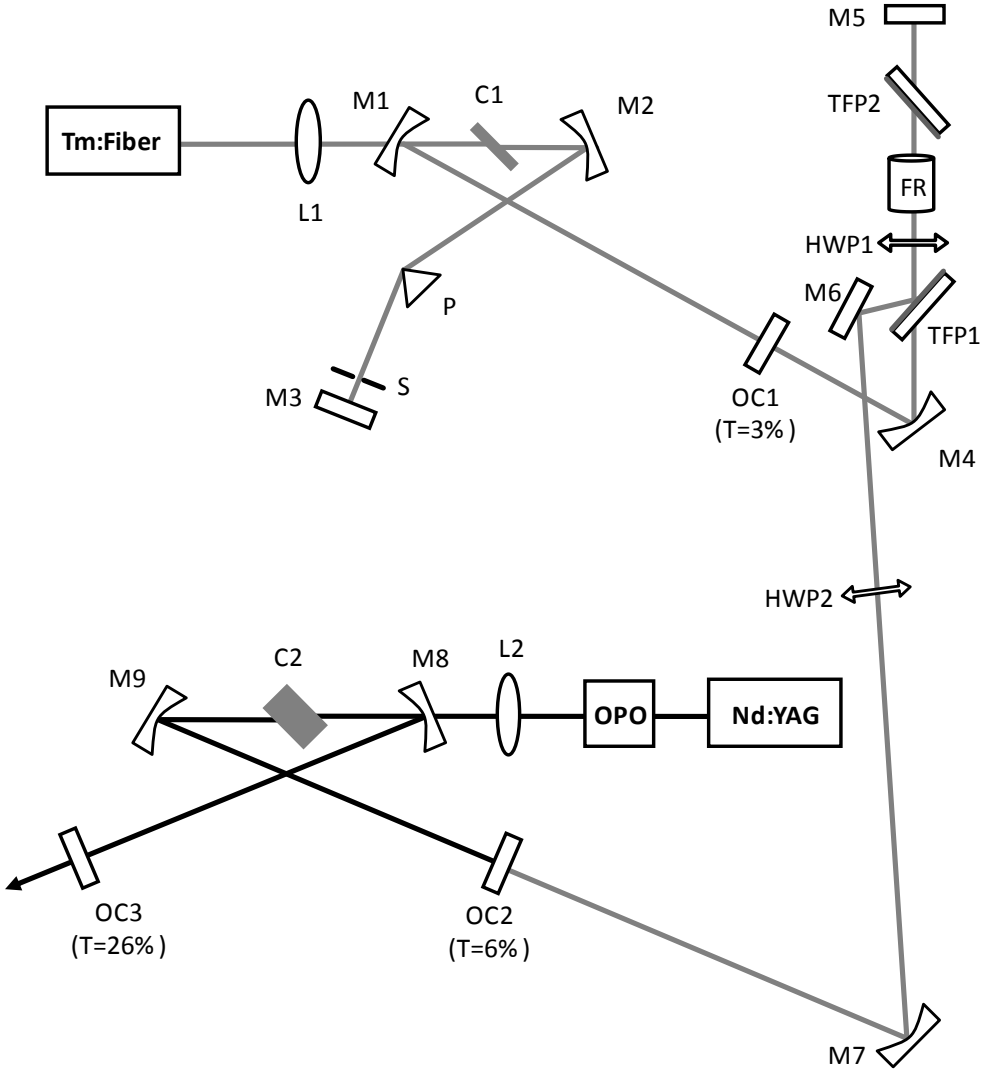

Figure 5.1: Injection-seeded Cr:ZnSe laser setup.

The output of the isolator was then directed with a flat aluminum mirror (M6) to the gain-switched oscillator. A curved high reflector (M7, radius of curvature=4 m) was further used to control the mode-matching between the CW and gain-switched Cr:ZnSe lasers.

With a second half--wave plate (HWP2), the polarization of the seed beam was adjusted to match the polarization of the beam emerging from the gain-switched oscillator. The x-type resonator of the gain-switched laser consisted of two curved mirrors (M8 and M9, radius of curvature=20 cm) and two flat output couplers having transmission values of 6 and 26 % (OC2 and OC3 in Fig. 1, respectively). The output coupler OC2 was used to couple the CW lseed beam into the gain-switched resonator while the injection-seeded output was taken from OC3 l. Inside the gain-switched resonator, a 6.6mm long polycrystalline Cr:ZnSe (C2) sample was used at Brewster incidence. The crystal had a small-signal absorption of 92 % at the pump wavelength of 1570 nm. The gain-switched Cr:ZnSe oscillator was pumped by a 1570-nm optical parametric oscillator (OPO), which, in turn, was pumped by a Q-switched Nd:YAG laser at 1064 nm. The pump pulsewidth (FWHM) and the pulse repetition rate were 50 ns and 1 kHz, respectively, during the experiments. The OPO pump beam was focused inside the crystal with a lens (L2) having a focal length of 20 cm. During the experiments, the spectrum of the gain-switched pulses was measured with a Czerny-Turner type, 0.5-m monochromator which had a resolution of 0.05 nm.

5.3 Injection Seeding Results and Discussion

Figure 5.2 shows the spectra of unseeded and seeded gain-switched Cr:ZnSe laser for three different seed wavelengths. In the absence of CW seed laser, the gain-switched oscillator had an output spectral width (FWHM) of 125 nm centered around 2360 nm. When the CW

laser beam was injected into the gain-switched laser cavity, the spectral width was narrowed down to 0.65 nm. In other words, the spectral brightness of the laser was improved by a factor of 192. In addition, we observed a strong dependence of linewidth of the injection-seeded laser on the CW laser spectrum. In the absence of an adjustable slit inside the CW laser cavity, the linewidth of the CW laser was broader and spectral hopping became very significant. In this case, the spectral linewidth of the injection-seeded laser increased to around 2 nm and additional parasitic spikes on the spectrum could be observed. By adjusting the slit width to reduce the linewidth of the CW laser to below 1 nm, we could eliminate the parasitic spikes and spectral jitter in the output of the gain-switched laser. During the spectrum measurements, the input pump pulse energy was around 600 μJ that was giving laser pulse energy between 100 and 130 μJ depending on the wavelength of the seed laser. In the experiments, the gain switched laser was seeded with the incident CW laser power of 1 to 5 mW on the output coupler, OC2. Below 1 mW of seed power, residual unseeded spectrum reapperead.

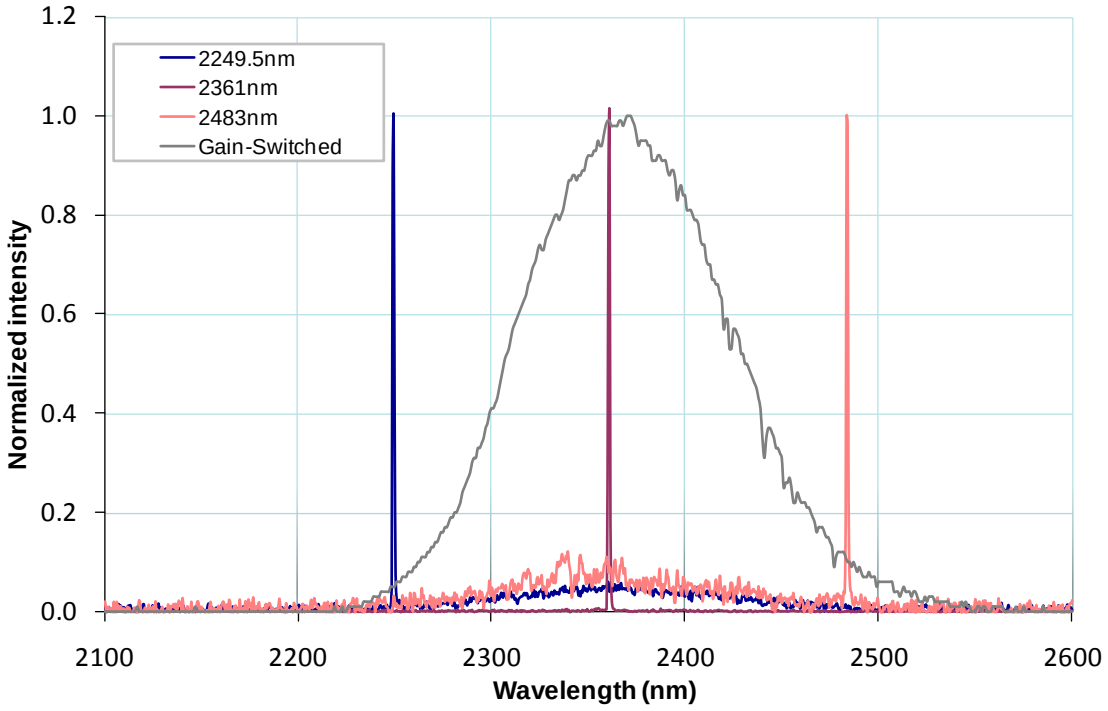

Figure 5.2: Unseeded and injection-seeded Cr:ZnSe laser spectra. The laser could be tuned between 2255 nm and 2455 nm.

The wavelength of the injection-seeded laser could be varied in the range of 2250-2483 nm by tuning the CW seed laser. When the CW laser was tuned to the two edges of the unseeded gain-switched laser spectrum, residual unseeded laser spectrum also reappeared (see Fig.5.2). This was due to the relatively low level of gain at the edges of the tuning range, preventing effective injection seeding. Figure 5.3 further shows the tuning curve of the injection-seeded Cr:ZnSe laser between 2255 and 2455 nm. In this spectral range, the residual unseeded gain-switched laser spectrum was not present. The

measurements were made at the incident pump energy of 600 μJ. The highest pulse energy was obtained at 2360 nm which was also the wavelength of peak emission from the unseeded gain-switched Cr:ZnSe laser. For both seeded and unseeded cases, the temporal pulse duration of the laser was measured to be around 30 ns.

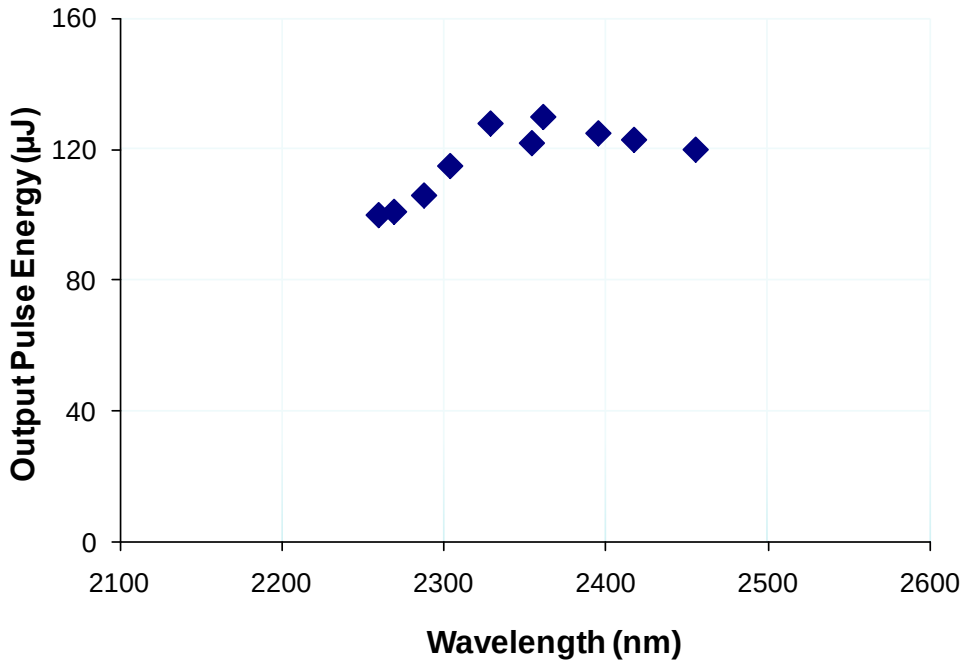

Figure 5.3: Tuning curve of injection-seeded Cr:ZnSe laser.

Figure 5.4 shows the efficiency curves of the unseeded and injection-seeded Cr:ZnSe laser. The output pulse energy was measured after the 26 % output coupler (OC3). The slope efficiency of the unseeded GS laser was determined to be 22.5 % with respect to the incident pump energy. By comparing the slope efficiencies at different output coupling

levels, the passive loss of the cavity was further found to be 5.6 %. Above 480 μJ of incident pump energy, saturation was observed in the output energy of the unseeded oscillator. That is due to the depletion of the ground-state population, resulting in a reduction of the pump absorption. However in the case of the injection-seeded laser, this saturation effect was observed at a higher incident pump energy (598 μJ). In the case of injection seeding, gain-switched laser pulses evolve from the seed laser light rather than noise. Hence, this reduces the time required for pulse formation. As a result, a higher rate of stimulated emission, initiated by the evolving laser pulse replenishes the ground-state population and reduces the saturation of pump absorption.

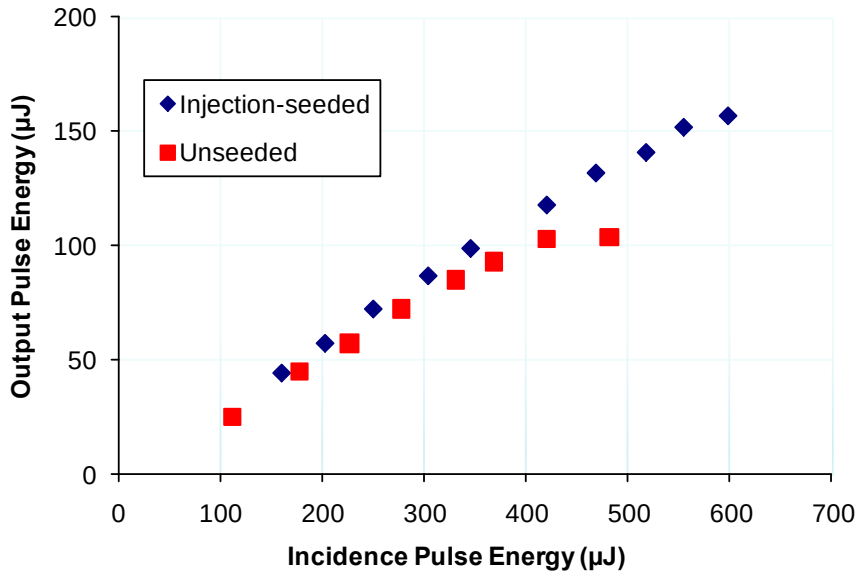

Figure 5.4: Efficiency curve of the injection-seeded and unseeded Cr:ZnSe laser as a function of incidence pump pulse energy.

5.4 Summary

In summary, we described a proof-of-principle experiment to reduce the spectral linewidth of a gain-switched Cr:ZnSe laser by CW injection seeding. An important advantage of the proposed scheme is that intracavity wavelength selective elements are not introduced into the gain-switched oscillator and hence additional losses are not introduced. Furthermore, because the saturation of pump absorption is reduced, higher output energy can be obtained from the oscillator in comparison with the unseeded case. In the experiments, the seeded Cr:ZnSe oscillator could be tuned between 2255 and 2455 nm by tuning the CW seed laser with an intracavity prism. The linewidth of the laser was further reduced from 125 nm to 0.65 nm during injection seeding. The laser could produce as high as 157 μJ-pulses with 598 μJ of incident pump energy at 1 kHz repetition rate. In principle, the spectral brightness of the seeded laser can be further improved by introducing additional wavelength selective elements into the CW laser cavity such as etalons.

Chapter 6

CHARACTERIZATION OF TWO-PHOTON ABSORPTION IN CdTe-CdS QUANTUM DOTS

6.1 Introduction

Multiphoton microscopy is an important in vivo technique in which the resolution of the image can be improved beyond the diffraction limit of the pump light. In this method, a fluorescent agent having no linear absorption but multiphoton absorption at the pump laser wavelength is injected into the tissue to be imaged. Then, a femtosecond laser light having a Gaussian beam shape is focused into the tissue. Since multiphoton process is strongly dependent on the intensity of the light, only the fluorescence agents experiencing high intensity light over a small portion of the Gaussian beam in the focus can absorb pump photons to emit light. By this way, it is possible to get images below the diffraction limit of the pump laser beam. Organic dye molecules are very commonly used as multi-photon fluorescent agents in multiphoton microscopy. Nowadays, quantum-dots (q-dot's) are preferred as the fluorescent agents in multiphoton microscopy because they have large two-photon cross-sections 100-1000x that of organic dyes which allows deeper tissue imaging

[92-93]. CdTe q-dots are the most promising fluorescent agents with respect to $CdS_{1-x}Se_x$ q-dot's [94]. Recent studies showed that CdTe-CdS core-shell q-dot architecture enhances quantum efficiency in the linear regime [95]. To the best of our knowledge, the two-photon absorption characteristics of core-shell CdTe-CdS q-dot's have not been investigated yet.

In this part of the thesis, we will analyze two-photon absorption and resulting emission process of core-shell CdTe-CdS q-dots. The emission spectra of the q-dot sample when pumped at 400 nm and 805 nm are almost identical. We showed that the emission efficiency was independent of the wavelength of the pump laser in the range of 740-860 nm. Furthermore, we determined the luminescence efficiency to be 60.7 % with respect to Rodamin 6G. In addition two-photon absorption cross-section was found out to be 4.1×10^6 GM which is much higher than that for standard CdTe q-dots.

6.2 Experimental

The water soluble CdTe-CdS q-dot sample was prepared by Esra Sevinç under the supervision of Dr. Havva Funda Yağcı Acar. The detailed description of the structure and synthesis of the q-dot's were discussed in Ref. [96]. The absorption spectrum of the sample was recorded by using a commercial UV-Vis-NIR spectrophotometer (Schimadzu, model 3101 PC) in the 200-1000 nm range. To investigate the two-photon optical process of the CdTe-CdS q-dot's, the sample was excited at the wavelength of 805 nm by using a home-made, tunable Ti:Sapphire laser where sample has no linear absorption. The laser was

operated in gain-switched regime at a pulse repetition rate of 1 kHz and produced 145-μJ, 60-ns pulses. The laser output was focused inside the q-dot sample by using a lens with focal length of 5 cm to a spotsize of 17 μm. The spotsize measurement was performed with a standard knife edge technique. The emission spectrum under two-photon excitation was measured by a commercial Czerny-Turner type monochromator (CVI, model DK 480) coupled with a photomultiplier tube (PMT) and a lock-in amplifier. We also recorded the emission due to the linear absorption at 400 nm by using a commercial photoluminescence spectrometer (Horiba, Flouromax-3) to compare with the emission spectrum due to two-photon absorption process. The two-photon absorption cross-section of the sample was determined by using the well-known z-scan technique. In this method, a pump laser beam was focused inside the sample and the transmission of the pump light through the sample was measured as a function of sample position around the focus. In the z-scan measurements, we used a multipass cavity, Kerr-lens mode-locked Ti:Sapphire laser producing pulses with 5-nJ pulse-energy and 112-fs pulse-duration. The spectrum of the laser was centered around 780 nm with a spectral width of 7 nm. The output of the laser was focused inside the sample with a 5cm-lens. The beam waist of the pump was measured to be 42 μm by using again the knife-edge technique. Figure 6.1 shows the picture of the mode-locked Ti:Sapphire laser and the z-scan measurement setup.

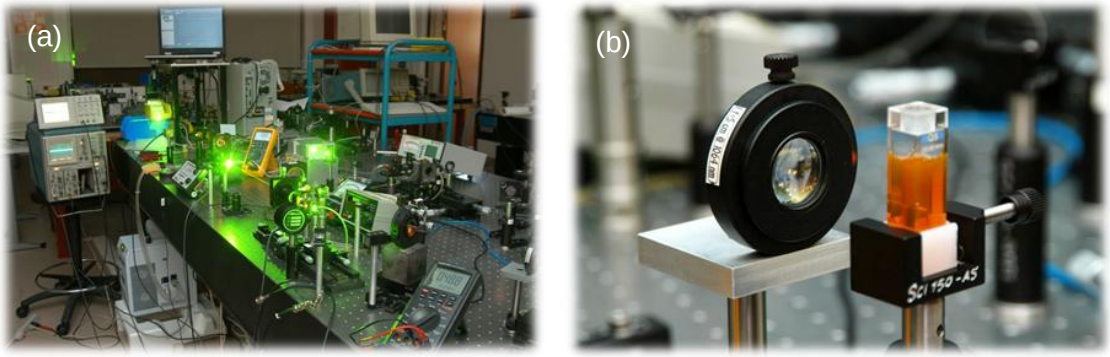

Figure 6.1: The pictures of (a) the mutipass-cavity femtosecond Ti:Sapphire laser and (b) the z-scan measurement setup.

6.3 Spectroscopy Results and Discussion

Figure 6.2 shows the absorption spectrum of the CdTe-CdS core-shell q-dot's in water. As can be seen from the absorption spectrum, the sample has two bands around 400 and 550 nm. Furthermore, the sample has almost no absorption around 800 nm where we excited.

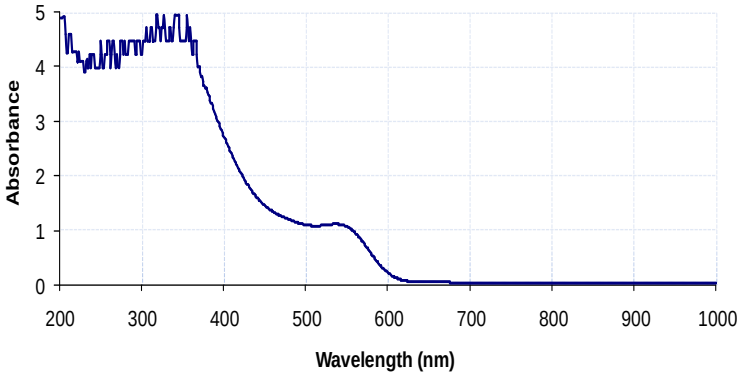

Figure 6.2: The absorption spectrum of the CdTe-CdS q-dot sample.

Figure 6.3 shows the emission spectrum of the sample excited at 800 nm and 400 nm. As can be seen, the emission spectra corresponding to the two excitation wavelengths are almost identical. Both emission spectra were centered around 588 nm. The peak at 532 nm on the emission spectrum with 805 nm excitation was due to unavoidable pump laser of the Ti:Sapphire laser.

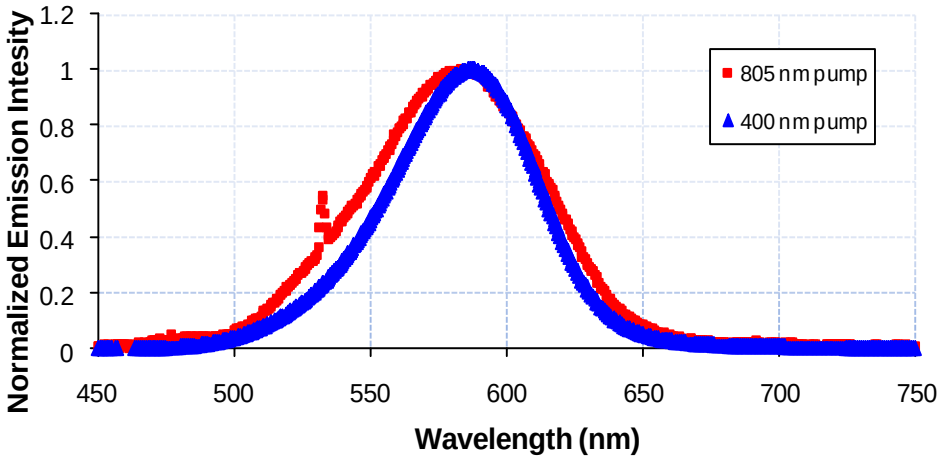

Figure 6.3: The emission spectrum of the CdTe-CdS q-dot sample excited at 400 and 805 nm.

As it is mentioned before, the two-photon absorption is a nonlinear process which has a quadratic dependence on the intensity of the pump light. The well known model for this process will be described in this chapter later. Since there is a quadratic dependence on pump photon intensity of the two photon absorption process, the emission intensity has very similar behavior as well. In order to investigate the relation between the emission and

pump intensity, the luminescence signal with excitation at 805 nm was measured as a function of incident pump peak power. During the measurements the same experimental setup for two-photon luminescence measurements was used. The wavelength of the monochromator was adjusted to the peak emission wavelength (588 nm). As can be seen from Figure 6.4, the emission intensity has a quadratic dependence with a linear term. A quadratic fit to the curve was also demonstrated in Figure 6.4. We believe that the linear term can be attributed to reabsorbtion of the emitted light due to presence of linear absorption band in the visible region.

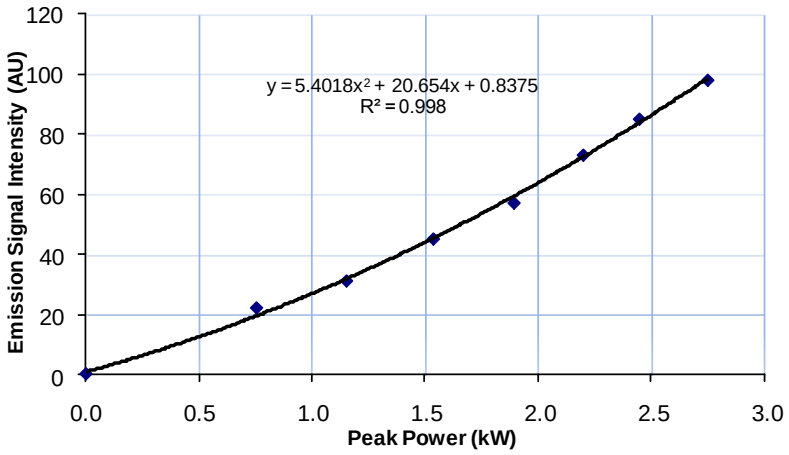

Figure 6.4: The emitted photon intensity of the CdTe-CdS q-dot sample at the wavelength of 588 nm as a function of incident pulse peak power. The wavelength of the pump laser was 805 nm.

We further investigated the emitted photon intensity as a function of pump wavelength using the same experimental setup in fluorescence measurement. As can be seen from Figure 6.5, the emitted photon intensity was not dependent on the pump photon wavelength in the range of 740-855nm. During the measurements, the laser wavelength was tuned by keeping the average laser power constant at 80 mW incident on the focusing lens (corresponds to 74 mW inside the sample holder).

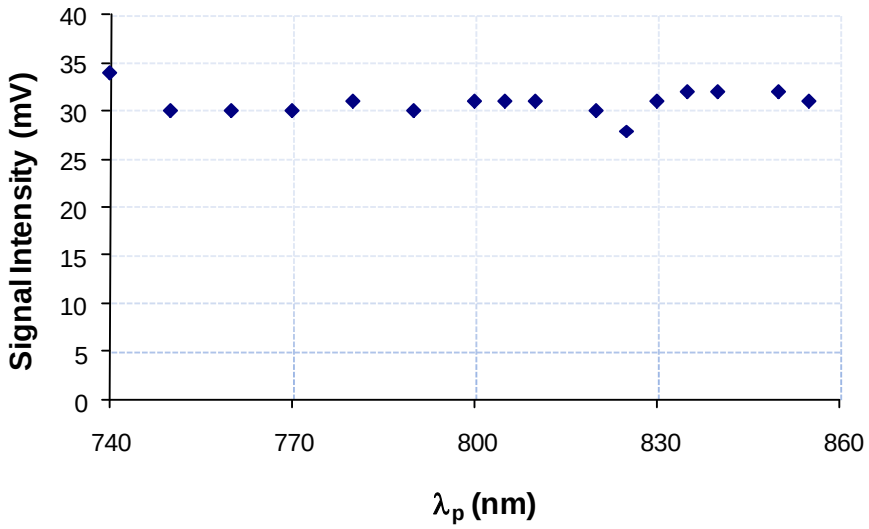

Figure 6.5: The emitted photon intensity of the CdTe-CdS q-dot sample at the wavelength of 588 nm as a function of pump photon wavelength. The average laser pump power was kept at 80 mW during the measurements.

In order to determine the absolute luminescence efficiency resulting from the two-photon absorption phenomena, we measured the spectrum of Rodamin 6G and q-dot sample having equal absorbance at 400 nm without any significant change on the

experimental setup. The integrated emission intensity of Rodamin 6G and the q-dot sample was determined by calculating the area under the emission spectrum. Then, the luminescence efficiency was calculated to be 60.7 % by calculating the ratio of the integrated emission intensity of the q-dot sample to that of Rodamin 6G. .

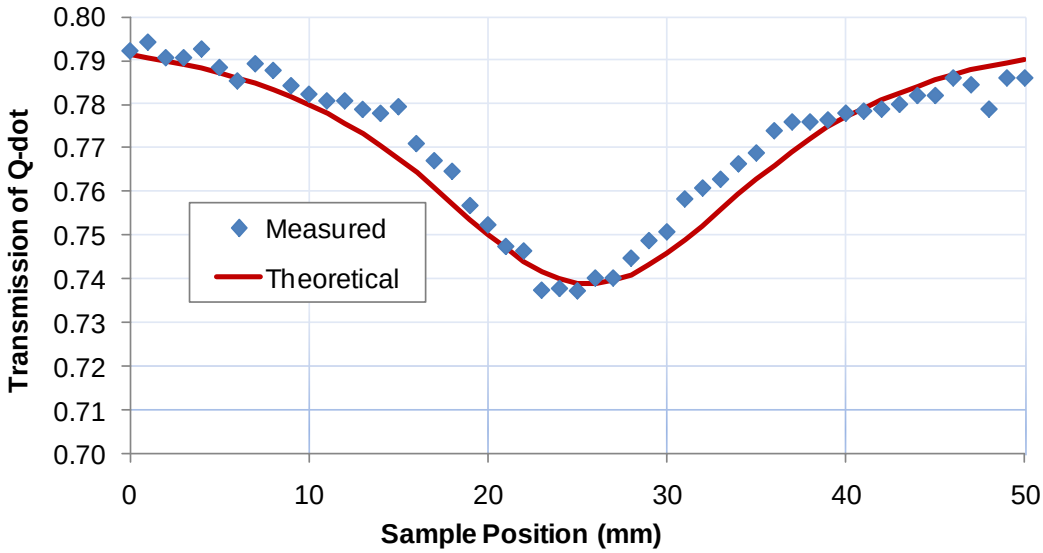

Figure 6.6: Z-scan measurement of the CdTe-CdS q-dot sample at the wavelength of 788 nm.Here, the transmission of the sample was measured as a function of sample position.

To compare the two-photon absorption strength of the core-shell CdTe-CdS q-dot's with the CdTe quantum-dots independent of the q-dot concentration, we determined the two-photon absorption cross-section (σ_{TPA}). The cross-section value was calculated from the two-photon absorption coefficient (β) which was derived from the z-scan measurement. Figure 6.6 shows the experimentally measured z-scan data where the

transmission of the q-dot solution was measured as a function the sample position around the focal point of the femtosecond laser beam. To determine β, a theoretical curve was fitted to the experimental data. The absorption of the pump beam in the presence of linear and two-photon absorption can be modeled by using the equation [97],

$$\frac{1}{I_p}\frac{\partial I_p}{\partial z} = -\alpha - \beta I_p. \tag{6.1}$$

Here α is the linear absorption coefficient (or, in general, the attenuation coefficient if there are other sources of loss such as scattering) at the pump wavelength, I_p is the pump photon intensity and z is the distance along the direction of propagation. The relationship between σ_{TPA} and β is given as,

$$\sigma_{TPA} = \rho^{-1}\frac{hc}{\lambda_p}\frac{\beta}{N}, \tag{6.2}$$

where ρ is Maxwell-Garnet local field correction factor ($\rho = 0.3$ for our case [98]), h is the Planck constant, c is the speed of light, λ_p is the pump wavelength and N is the q-dot concentration in the solution. In this study, N is determined to be $5.7\text{x}10^{15}$ cm^{-3} from the absorption spectrum of the sample by using an empirical equation for the concentration in Ref [99] derived for CdTe q-dot's. Here, there is an unknown uncertainty in the value of N since the empirical formula used was determined for standard CdTe q-dots not for core-shell quantum dots.

Table 6.1 summarizes the σ_{TPA} and β values for CdTe and CdSe q-dot's reported in the literature. As can be seen, the σ_{TPA} values vary between 7.96×10^3-9×10^4 GM (Goeppert-Mayer, $1GM=10^{-50}\,cm^4\,sec\,photon^{-1}$) depending on the q-dot synthesis technique and conditions. In this study, σ_{TPA} for core-shell structured q-dot's was found to be 4.1×10^6 GM which is much higher than the reported values. We believe that the improvement in the cross-section is due to enhanced quantum confinement effect withthe introduction of the shell structure. That also leads an increase in quantum efficiency which is reported for linear optical processes in q-dots [95]. Even though σ_{TPA} value for core-shell structured q-dot sample is relatively higher, we have encountered a reproducibility problem with the sample. A possible reason behind this problem might be uncontrolled oxidation of Te source during synthesis. That might also affect the size of the core as well as the shell, leading to a shift in the wavelength of optimum two-photon absorption. The femtosecond Ti:sapphire source used in our experiments could only be operated at the fixed wavelength of 788 nm. The problem requires further investigation and optimization of the synthesis.

Q-dot	β (cm/W)	σ_{TPA} (GM)	Reference
CdTe in toluene	-	7.96×10^{3}	[100]
CdTe	6.4×10^{-8}	-	[101]
CdSe-ZnS	-	4.7×10^{4}	[102]
CdTe	6.1×10^{-8}	1.7×10^{4}	[103]
CdTe	-	10^{4}-10^{5}	[104]
CdTe	-	8×10^{4}-9×10^{4}	[98]
CdSe	-	6×10^{4}	[98]
CdTe-CdS	1.4×10^{-10}	4.1×10^{6}	In this study

Table 6.1: Summary of the the two-photon absorption cross-section and absorption coefficient valuesreported in the literature for CdTe ans CdSe q-dots.

6.4 Summary

In summary, we analyzed the two-photon absorption and emission properties of core-shell CdTe-CdS q-dots. We showed that emission strength of the sample was independent of the wavelength of the pump laser in the range of 740-860 nm. Moreover, we found out that the luminescence quantum efficiency was 60.7 % with respect to that of Rodamin 6G. Furthermore, the two-photon absorption cross-section was determined to be 4.1×10^{6} GM. We encountered a reproducibility problem in the z-scan measurements which suggest that further investigation is needed to optimize the synthesis of the core-shell structures.

Chapter 7

CONCLUSIONS

In this thesis, we focused on the development of advanced near and mid-infrared pulsed lasers and their application in the characterization of two-photon absorption properties of quantum dots. In particular, we discussed the development of solitary and chirped-pulse Cr^{4+}:Forsterite laser, Nd doped tellurite glass laser, continuous-wave injection-seeded gain-switched Cr:ZnSe laser and the application of Multi-pass cavity femtosecond Ti:sapphire lasers in the optical characterization of CdTe-CdS core-shell quantum dots.

First, we experimentally demonstrated the mode-locked operation of a low-threshold, room-temperature, multipass-cavity femtosecond Cr^{4+}:Forsterite laser. The repetition rate was lowered to 11.7 MHz by using a q-preserving multipass cavity. Mode-locking was sustained by using the Kerr-lens mode-locking technique. As high as 5.1-nJ, nearly transform-limited pulses with a duration of 68 fs were generated at an output power of only 60 mW. Furthermore, as short as 41-fs pulses could be obtained with a pulse energy of 3.4 nJ at an absorbed pump power of 1.1 W [55]. In the positive dispersion regime, we obtained record 81-nJ pulses directly from the Cr^{4+}:Forsterite oscillator operating at 4.9

MHz [60]. In that case, pulse duration at the output of the laser was 5.5 ps. By using an external compression system, the pulses were then be compressed to 607 fs. High-energy mode-locked oscillators operating in this wavelength range should be important in various biomedical applications including deep-tissue multi-photon microscopy as well optical coherence tomography.

Second, lasing in a novel, neodymium-doped tellurite-based glass with the host composition $(0.8)TeO_2$-$(0.2)WO_3$ was demostrated. To our best knowledge, this is the first time laser operation from Nd:Tellurite glass with this composition was reported in the literature [23]. During gain switched operation, the glass laser produced 11 μJ of output energy at 1065 nm with 114 μJ of pump. The slope efficiency with respect to incident energy was 12%. Then, laser operation at 1370 nm of the same glass sample was demonstrated. To our best knowledge, this is the first lasing action demonstrated in the literature, at 1370 nm in a bulk tellurite glass for the energy transition $^4F_{3/2} \rightarrow {}^4I_{13/2}$ of the Nd^{3+} ion [22]. The laser was operated in the gain-switched regime at 1 kHz with a threshold pulse energy of 59 μJ. The slope efficiency was further determined to be 5.5 %. As high as 6μJ-pulses with a duration of 1.74 μs were obtained. From the threshold analysis, the emission cross section came to 1.57×10^{-20} cm^2 in the presence of excited-state absorption. In addition, the excited-state absorption cross section, σ_{ESA} was estimated to be 1.22×10^{-20} cm^2 by using the slope efficiency analysis. These results indicate that

doped tellurite glasses have the potential of being used in the development of efficient bulk glass lasers and fiber lasers.

Then, we described a proof-of-principle experiment to reduce the spectral linewidth of a gain-switched Cr:ZnSe laser by CW injection seeding [91]. An important advantage of the proposed scheme is that intracavity wavelength selective elements are not introduced into the gain-switched oscillator and hence additional losses are not introduced. In the experiments, the seeded Cr:ZnSe oscillator could be tuned between 2255 and 2455 nm by tuning the CW seed laser with an intracavity prism. The linewidth of the laser was further reduced from 125 nm to 0.65 nm during injection seeding. The laser could produce as high as 157 μJ-pulses with 598 μJ of incident pump energy at 1 kHz repetition rate. In principle, the spectral brightness of the seeded laser can be further improved by introducing additional wavelength selective elements into the CW seed laser such as etalons.

Finally, we demonstrated an application of a multipass-cavity femtosecond Ti:sapphire laser in the optical characterization of quantum dots. In particular, we analyzed the two-photon absorption and resulting emission of core-shell CdTe-CdS q-dots. We showed that the emission strength of the sample was independent of the wavelength of the pump laser in the range of 740-860 nm. Moreover, we found out that the luminescence quantum efficiency was 60.7 % with respect to that for Rodamin 6G. Furthermore, the two-photon absorption cross-section was determined to be 4.1×10^6 GM. We encountered reproducibility issues in the z-scan measurements repeated with other samples, suggesting

that further investigation may be necessary to optimize the synthesis of the core-shell quantum dots.

BIBLIOGRAPHY

1. Maiman, T.H., *Stimulated optical radiation in ruby.* Nature, 1960. **187**(4736): p. 493-494.
2. Kao, K.C. and T.W. Davies, *Spectrophotometric studies of ultra low loss optical glasses – I: Single beam method.* Journal of Physics E, 1968. **2**(1): p. 1063.
3. Eckstein, J.N., A.I. Ferguson, and T.W. Hänsch, *High-resolution two-photon spectroscopy with picosecond light pulses.* Physical Review Letters, 1978. **40**(13): p. 847–850
4. Yablonovitch, E., *Inhibited Spontaneous Emission in Solid-State Physics and Electronics.* Physical Review Letters, 1987. **58**(20): p. 2059–2062.
5. John, S., *Strong localization of photons in certain disordered dielectric superlattices.* Physical Review Letters, 1987. **58**(23): p. 2486–2489.
6. Denk, W., J.H. Strickler, and W.W. Webb, *Two-Photon Laser Scanning Fluorescence Microscopy.* Science, 1990. **248**(4951): p. 73-76.
7. Weber, M.J., *Handbook of laser wavelengths*. 1999, Boca Raton: CRC Press.
8. Sorokin, E., *Solid-state materials for few-cycle pulse generation and amplification*, in *Few-cycle laser pulse generation and its applications*, F.X. Kartner, Editor. 2004, Springer-Verlag: Berlin. p. 3-71.
9. Valdmanis, J.A., R.L. Fork, and J.P. Gordon, *Generation of optical pulses as short as 27 fs directly from a laser balancing self-phase modulation, group-velocity dispersion, saturable absorption, and saturable gain.* Optics Letters, 1985. **10**: p. 131-133.
10. Paschotta, R. and U. Keller, *Passively Mode-Locked Solid-State Lasers*, in *Solid-State Lasers and Applications*, A. Sennaroglu, Editor. 2007, Taylar & Francis: Boca Taton. p. 259-318.

11. Keller, U. and A.C.Tropper, *Passively mode-locked surface emitting semiconductor lasers* Physics Reports, 2006. **429**: p. 67-120.
12. Jackson, S.D., *Single-transverse-mode 2.5-W holmium-doped flouride fiber laser operating at 2.86 um.* Optics Letters, 2004. **29**(4): p. 334-336.
13. Jackson, S.D. and T.A. King, *Efficient gain-switched operation of a Tm-doped silica fiber laser.* IEEE Journal of Quantum Electronics, 1998. **34**(5): p. 779-789.
14. Jeong, Y., et al., *Ytterbium-doped large-core fiber laser with 1.36 kW continuous-wave output power.* Optics Express, 2004. **12**(25): p. 6088-6092.
15. Becker, C., et al., *Advanced Ti:Er:LiNbO3 waveguide lasers.* IEEE Journal on Selected Topics in Quantum Electronics, 2000. **6**(1): p. 101 - 113
16. Calmano, T., et al., *Nd:YAG waveguide laser with 1.3 W output power, fabricated by direct femtosecond laser writing.* Applied Physics B, 2010. **100**(1): p. 131-135.
17. Eggleston, J.M., et al., *The Slab Geometry Laser-Part I: Theory.* IEEE Journal of Quantum Electronics, 1984. **20**(3): p. 289-301.
18. Albrecht, G.F., J.M. Eggleston, and J.J. Ewing, *Design and Characterization of a High Average Power Slab YAG Laser.* IEEE Journal of Quantum Electronics, 1986. **22**(11): p. 2099-2106.
19. Zhu, P., et al., *Diode end-pumped high-power Q-switched double Nd:YAG slab laser and its efficient near-field second-harmonic generation.* Optics Letters, 2008. **33**(19): p. 2248-2250.
20. Baer, C.R.E., et al., *Femtosecond Yb:Lu2O3 thin disk laser with 63 W of average power.* Optics Letters, 2009. **34**(18): p. 2823-2825.
21. Neuhaus, J., et al., *Passively mode-locked Yb : YAG thin-disk laser with pulse energies exceeding 13 mu J by use of an active multipass geometry.* Optics Letters, 2008. **33**(7): p. 726-728.

22. Cankaya, H. and A. Sennaroglu, *Bulk Nd^{3+}-doped tellurite glass laser at 1.37 μm.* Applied Physics B-Lasers and Optics, 2010. **99**: p. 121-125.

23. Kalaycioglu, H., et al., *Lasing at 1065 nm in bulk Nd^{3+}-doped telluride-tungstate glass.* Optics Communications, 2008. **281**(24): p. 6056-6060.

24. Snitzer, E., *Optical Maser Action of Nd^{+3} in A Barium Crown Glass.* Physical Review Letters, 1961. **7**(12): p. 444-446.

25. Snitzer, E., *Glass Lasers.* Applied Optics, 1966. **5**(10): p. 1487-1499.

26. Kaminskii, A.A., *Crystalline lasers: physical processes and operating schemes*. Laser and optical science and technology series, ed. M.J. Weber. 1996, New York: CRC.

27. Kaminskii, A.A., *Laser crystals and ceramics: recent advances.* Laser & Photon. Rev., 2007. **1**(2): p. 93-177.

28. Taira, T., *Ceramic YAG lasers.* Comptes Rendus Physique

Recent advances in crystal optics, 2007. **8**(2): p. 138-152.

29. Kalisky, Y., *Cr^{4+}-doped crystals: their use as lasers and passive Q-switches.* Progress in Quantum Electronics, 2004. **28**: p. 249-303.

30. Fischer, C., et al., *Photoacoustic monitoring of gases using a novel laser source tunable around 2.5 μm.* Optics and Lasers in Engineering, 2005. **43**: p. 573-582.

31. Morgner, U., et al., *Sub-two-cycle pulses from a Kerr-lens mode-locked Tisapphire laser.* Optics Letters, 1999. **24**(6).

32. Wagner, G.J., et al. *Single-Frequency Cr:ZnSe Laser*. in *OSA Advanced Solid-State Photonics*. 2004. New Mexico: OSA.

33. Barnes, J.C., et al., *Injection Seeding II: Ti :A120, Experiments.* IEEE Journal of Quantum Electronics, 1993. **29**(10): p. 2684-2692.

34. Sutter, D.H., et al., *Semiconductor saturable-absorber mirror-assisted Kerr-lens mode-locked Ti : sapphire laser producing pulses in the two-cycle regime.* Optics Letters, 1999. **24**(9): p. 631-633.
35. Keller, U., et al., *Semiconductor saturable absorber mirrors (SESAM's) for femtosecond to nanosecond pulse generation in solid-state lasers.* IEEE Journal of Selected Topics in Quantum Electronics, 1996. **2**(3): p. 435-453.
36. Haus, H.A., *Mode-Locking of Lasers.* IEEE Journal of Quantum Electronics, 2000. **6**: p. 1173-1185.
37. Kærtner, F.X., Matuschek, N., Schibli, T., Keller, U., *Design and fabrication of double-chirped mirrors.* Optics Letters, 1997. **22**(1): p. 831-833.
38. Golubovic, B., et al., *Double Gires—Tournois interferometer negative-dispersion mirrors for use in tunable mode-locked lasers.* Optics Letters, 2000. **25**(4): p. 275-277.
39. Naumov, S., et al., *Approaching the microjoule frontier with femtosecond laser oscillators.* New Journal of Physics, 2005. **7**: p. 216-226.
40. Proctor, B., E. Westwig, and F. Wise, *Characterization of a Kerr-Lens Mode-Locked Ti-Sapphire Laser with Positive Group-Velocity Dispersion.* Optics Letters, 1993. **18**(19): p. 1654-1656.
41. Kalashnikov, V.L., et al., *Chirped-pulse oscillators: theory and experiment.* Applied Physics B-Lasers and Optics, 2006. **83**(4): p. 503-510.
42. Siegel, M., et al., *Microjoule pulse energy from a chirped-pulse Ti:sapphire oscillator with cavity dumping.* Optics Letters, 2009. **34**(6): p. 740-742.
43. Dewald, S., et al., *Ionization of noble gases with pulses directly from a laser oscillator.* Optics Letters, 2006. **31**(13): p. 2072-2074.
44. Tearney, G.J., et al., *In vivo endoscopic optical biopsy with optical coherence tomography.* Science, 1997. **276**: p. 2037-2039.

45. Spielmann, C., et al., *Generation of coherent x-rays in the water window using 5-femtosecond laser pulses.* Science, 1997. **278**: p. 661-664.

46. Drescher, M., et al., *Time-resolved atomic inner-shell spectroscopy.* Nature, 2002. **419**(6909): p. 803-807.

47. Herriot, D., H. Kogelnik, and R. Kompfner, *Off-Axis in Spherical Mirror Interferometers.* Applied Optics, 1964. **3**(4): p. 523-526.

48. Cho, S.H., Bouma, B.E., Ippen, E.P., Fujimoto, J.G., *Low-repetition-rate high-peak-power Kerr-lens mode-locked Ti:Al_2O_3 laser with a multiple-pass cavity.* Optics Letters, 1999. **24**(6): p. 417-419.

49. Sennaroglu, A. and J.G. Fujimoto, *Design criteria for Herriott-type multi-pass cavities for ultrashort pulse lasers.* Optics Express, 2003. **11**: p. 1106-1113.

50. Kowalevicz, A.M., et al., *Generation of 150-nJ pulses from a multiple-pass cavity Kerr-lens mode-locked Ti:Al2O3 oscillator.* Optics Letters, 2003. **28**(17): p. 1597-1599.

51. Sennaroglu, A., Kowalevicz, A. M., Kartner, F.X., Fujimoto, J.G., *High-performance, compact, prismless, low-thereshold 30-MHz Ti:Al_2O_3 laser.* Optics Letters, 2003. **28**(18): p. 1674-1676.

52. Prasankumar, R.P., et al., *An extended cavity femtosecond Cr:LiSAF laser pumped by low cost diode lasers.* Optics Express, 2003. **11**(11): p. 1265-1269.

53. Papadopulos, D.N., et al., *Passively mode-locked diode-pumped Nd:YVO4 oscillator operating at an ultralow repetition rate.* Optics Letters, 2003. **28**(19): p. 1838-1840.

54. Kolev, V.Z., et al., *Passive mode locking of a Nd : YVO4 laser with an extra-long optical resonator.* Optics Letters, 2003. **28**(14): p. 1275-1277.

55. Cankaya, H., J.G. Fujimoto, and A. Sennaroglu. *Efficient, low-threshold, multipass-cavity femtosecond Cr4+:forsterite laser*. in *Advanced Solid-State Photonics*. 2009. Denver, Colarado, USA: OSA.

56. Sennaroglu, A., et al., *Compact femtosecond lasers based on novel multi-pass cavities.* IEEE Journal of Quantum Electronics, 2004. **40**: p. 519-528.

57. Sennaroglu, A., F.X. Kaertner, and J.G. Fujimoto, *Low-threshold, room-temperature femtosecond Cr^{4+}:forsterite laser.* Optics Express, 2007. **15**(20): p. 13043-13048.

58. Liu, X., D. Du, and G. Mourou, *Laser ablation and micromachining with ultrashort laser pulses.* IEEE Journal of Quantum Electronics, 1997. **33**(10): p. 1706-1716.

59. Shcheslavskiy, V., V.V. Yakovlev, and A. Ivanov, *High-energy self-starting femtosecond Cr4+:Mg2SiO4 oscillator operating at a low repetition rate.* Optics Letters, 2001. **26**: p. 1999-2001.

60. Cankaya, H., A. Sennaroglu, and S. Akturk, *Direct generation of 81 nJ pulses and external compression to a subpicosecond regime with a 4.9 MHz chirped-pulse multipass-cavity Cr(4+):forsterite oscillator.* Optics Letters, 2011. **36**(9): p. 1572-1574.

61. Kartner, F.X., et al., *Design and fabrication of double-chirped mirrors.* Optics Letters, 1997. **22**(11): p. 831-833.

62. Huang, D., et al., *Self-Focusing-Induced Saturable Loss for Laser Mode-Locking.* Optics Letters, 1992. **17**(7): p. 511-513.

63. Chassagne, B., et al., *Experimental determination of the nonlinear refractive index in an operating Cr:forsterite femtosecond laser.* Optics Communications, 1997. **141**(1-2): p. 69-74.

64. Wang, J.S., E.M. Vogel, and E. Snitzer, *Tellurite glass: a new candidate for fiber devices.* Optical Materials, 1994. **3**: p. 187-203.

65. Sennaroglu, A., A. Kurt, and G. Özen, *Effect of cross relaxation on the 1470 and 1800 nm emissions in Tm^{3+}:TeO_2-$CdCl_2$ glass.* Journal of Physics: Condensed Matter, 2004. **16**: p. 2471-2478.

66. Sennaroglu, A., et al., *Spectroscopic properties of Tm^{3+}:TeO_2-PbF_2 glasses.* Journal of Luminescence, 2006. **116**: p. 79-86.

67. Iparraguirre, I., et al., *Laser action and upconversion of Nd^{3+} in tellurite bulk glass.* Journal of Non-Crystalline Solids, 2007. **353**(8-10): p. 990-992.

68. Moulton, P.F., *An Investigation of the Co:MgF_2 Laser System.* IEEE Journal of Quantum Electronics, 1985. **21**(10): p. 1582-1595.

69. Bouma, B.E., et al., *Self-phase-modulated Kerr-lens mode-locked Cr:forsterite laser source for optical coherence tomography.* Optics Letters, 1996. **21**(22): p. 1839-1841.

70. Petrin, R.R., et al., *Spectroscopy and Laser Operation of Nd-ZBAN Glass.* IEEE Journal of Quantum Electronics, 1991. **27**(4): p. 1031-1038.

71. De Camargo, A.S.S., et al., *Auger upconversion energy transfer losses and efficient 1.06 μm laser emission in Nd^{3+} supercript stop doped fluoroindogallate glass.* Applied Physics B-Lasers and Optics, 2006. **83**(4): p. 565-569.

72. Schweizer, T., et al., *Rare-earth doped chalcogenide glass laser.* Electronics Letters, 1996. **32**(7): p. 666-667.

73. De Sousa, D.F., et al., *Laser emission at 1077 nm in Nd^{3+}-doped calcium aluminosilicate glass.* Applied Physics B-Lasers and Optics, 2003. **77**(1): p. 59-63.

74. Fernandez, J., et al., *Laser action and upconversion of Nd^{3+} in lead-niobium-germanate bulk glass.* Optical Materials, 2004. **25**(2): p. 185-191.

75. Michel, J.C., D. Morin, and F. Auzel, *Proprietes spectroscopiques et effet laser d'un verre tellurite et d'un verre phosphate fortement dopes en neodyme.* Rev. Phys. Appl., 1978. **13**: p. 859-866.

76. Lei, N., B. Xu, and Z.H. Jiang, *Ti:sapphire laser pumped Nd:tellurite glass laser.* Optics Communications, 1996. **127**(4-6): p. 263-265.

77. Weber, M.J., J.D. Myers, and D.H. Blackburn, *Optical-Properties of Nd-$^{3+}$ in Tellurite and Phosphotellurite Glasses.* Journal of Applied Physics, 1981. **52**(4): p. 2944-2949.

78. Richards, B., et al., *Efficient ~2 μm Tm^{3+}-doped tellurite fiber laser.* Optics Letters, 2008. **33**(4): p. 402-404.

79. Hakimi, F., et al., *Glass-Fiber Laser at 1.36-μm from Sio2-Nd.* Optics Letters, 1989. **14**(19): p. 1060-1061.

80. Brierley, M., et al., *Amplification in the 1300 nm Telecommunications Window in a Nd-Doped Fluoride Fiber.* Electronics Letters, 1990. **26**(5): p. 329-330.

81. Miniscalco, W.J., et al., *1.3 μm Fluoride Fiber Laser.* Electronics Letters, 1988. **24**(1): p. 28-29.

82. Sennaroglu, A., C.R. Pollock, and H. Nathel, *Efficient continuous-wave chromium-doped YAG laser.* Journal of Optical Society of America B, 1995. **12**(5): p. 930-937.

83. Pelouch, W.S., et al. *Mid-Wave ZGP OPOs pumped by a Cr:ZnSe laser*. in *Advanced Solid State Photonics*. 2001. San Jose: OSA.

84. Bernhardt, B., et al., *Mid-infrared dual-comb spectroscopy with 2.4 μm Cr2+:ZnSe femtosecond lasers.* Applied Physics B-Lasers and Optics, 2010. **100**(1): p. 3-8.

85. Cankaya, H., et al., *Absorption saturation analysis of Cr2+: ZnSe and Fe2+: ZnSe.* Journal of the Optical Society of America B-Optical Physics, 2008. **25**(5): p. 794-800.

86. DeLoach, L.D., et al., *Transition Metal-Doped Zinc Chalcogenides Spectroscopy and Laser Demonstration of a New Class of Gain Media.* IEEE Journal of Quantum Electronics, 1996. **32**(6): p. 885-895.

87. Demirbas, U. and A. Sennaroglu, *Intracavity-pumped Cr^{2+}: ZnSe laser with ultrabroad tuning range between 1880 and 3100 nm.* Optics Letters, 2006. **31**(15): p. 2293-2295.

88. Page, R.H., et al., *Cr^{2+} Doped Zinc Chalcogenides as Efficient, Widely Tunable Mid-Infrared Lasers.* IEEE Journal of Quantum Electronics, 1997. **33**(4): p. 609-619.

89. Moskalev, I.S., V.V. Fedorov, and S.B. Mirov, *Tunable, single-frequency, and multi-watt continuous-wave Cr2+: ZnSe lasers.* Optics Express, 2008. **16**(6): p. 4145-4153.

90. Zhang, C.H., et al., *Efficient Cr:ZnSe laser with a volume Bragg grating.* Laser Physics, 2011. **21**(1): p. 44-47.

91. Cankaya, H., et al., *Efficient injection-seeded gain-switched tunable Cr:ZnSe laser* Optics Letters, Submitted.

92. Larson, D.R., et al., *Water-soluble quantum dots for multiphoton fluorescence imaging in vivo.* Science, 2003. **300**(5624): p. 1434-1436.

93. Voura, E.B., et al., *Tracking metastatic tumor cell extravasation with quantum dot nanocrystals and fluorescence emission-scanning microscopy.* Nature Medicine, 2004. **10**(9): p. 993-998.

94. Banfi, G.P., et al., *2-Photon Absorption in Semiconductor Nanocrystals.* Physical Review B, 1994. **50**(8): p. 5699-5702.

95. Bao, H.B., et al., *Enhancement effect of illumination on the photoluminescence of water-soluble CdTe nanocrystals: Toward highly fluorescent CdTe/CdS core-shell structure.* Chemistry of Materials, 2004. **16**(20): p. 3853-3859.

96. Seviç, E., *Development of Aqueous CdS and CdTe/CdS Quantum Dots via DMSA decomposition*, in *Materials Science and Engineering*. 2009, Koc University: Istanbul.

97. Sheikbahae, M., et al., *Sensitive Measurement of Optical Nonlinearities Using a Single Beam.* Ieee Journal of Quantum Electronics, 1990. **26**(4): p. 760-769.

98. Padilha, L.A., et al., *Frequency degenerate and nondegenerate two-photon absorption spectra of semiconductor quantum dots.* Physical Review B, 2007. **75**: p. 075325.

99. Yu, W.W., et al., *Experimental Determination of the Extinction Coefficient of CdTe, CdSe, and CdS Nanocrystals.* Chemistry of Materials, 2003. **15**(14): p. 2854-2860.

100. Pu, S.-C., et al., *The Empirical Correlation Between Size and Two-Photon Absorption Cross Section of CdSe and CdTe Quantum Dots.* Small, 2006. **2**(11): p. 1308 – 1313.

101. Tan, G.L., et al., *Linear and non-linear optical properties of capped CdTe nanocrystals prepared by mechanical alloying.* Optical Materials, 2004. **27**: p. 579–584.

102. Larson, D.R., et al., *Water-Soluble Quantum Dots for Multiphoton Fluorescence Imaging in Vivo.* Science, 2003. **300**: p. 1434-1436.

103. Pan, L., et al., *Nonlinear optical properties of thiol-capped CdTe quantum dots in nonresonant region.* Applied Physics Letters, 2007. **91**: p. 051902.

104. Pan, L., A. Ishikawa, and N. Tamai, *Detection of optical trapping of CdTe quantum dots by two-photon-induced luminescence.* Physical Review B, 2007. **75**: p. 161305.

VITA

Huseyin Cankaya was born in Isparta, Turkey in 1980. He received his BS degree in Physics in 2004 and MS degree in Materials Science and Engineering in 2006 from Koc University, Istanbul. He recently obtained his PhD degree in materials science and engineering from Koc University in 2011. He will continue his research in development of lasers and amplifiers for coherent x-ray generation as a postdoctoral associate in DESY, Hamburg. His current research includes development Cr:ZnSe lasers and amplifiers, the investigation of optical and lasing characteristics of rare-earth ion-doped tellurite glasses, the development of solitary and chirped-pulse Cr:forsterite, the optical characterization of colloidal quantum dots, Cr:ZnSe and Cr:YAG saturable-absorber characterization and application in passive q-switching, photoluminescence of Er doped polymers, lasing characteristics of microdroplets on a superhydrophobic surface.

Mr. Cankaya is an author and coauthor of more than 10 journal papers. He serves as a reviewer in Optics Letters, Optics Express, Journal of Optical Society of America B and International Journal of Modern Physics B. He is a member of Optical Society of America (OSA) and Institute of Electrical and Electronics Engineering (IEEE) Photonics Society.

JOURNAL ARTICLES

- Adil Tolga Gorgulu, **Huseyin Cankaya,** Adnan Kurt, , Adolfo Speghini, Marco Bettinelli and Alphan Sennaroglu, "Spectroscopic characterization of Tm^{3+}:TeO_2 - K_2O-Nb_2O_5 glasses for 2-μm lasing applications"**,** Journal of Luminescence, (in press).
- **Huseyin Cankaya,** Selcuk Akturk and Alphan Sennaroglu, "Direct generation of 81-nJ pulses and external compression to subpicosecond regime with a 4.9-MHz chirped-pulse multipass-cavity Cr^{4+}:forsterite oscillator", Optics Letters, 2011. **36**: p1572-1574.
- Yasin Karadag, Mustafa Gundogan, M.Yavuz Yuce, **Huseyin Cankaya**, Alphan Sennaroglu, and Alper Kiraz, "Prolonged Raman lasing in size-stabilized salt-water microdroplets on a superhydrophobic surface", Optics Letters, 2010. **35**: p1995-1997.
- **Huseyin Cankaya**, Reyhane Kilci, Alphan Sennaroglu, Emel Yilgor, Iskender Yilgor, "Erbium(III)-doped polyurethaneureas: Novel broadband ultraviolet-to-visible converter", Journal of Applied Polymer Science, 2010. **117**: p378-383.
- **Huseyin Cankaya** and Alphan Sennaroglu, "Bulk Nd^{3+}-doped tellurite glass laser at 1.37 μm", Applied Physics B, 2010. **99**: p121-125.
- M.Natali Cizmeciyan, **Huseyin Cankaya**, Adnan Kurt and Alphan Sennaroglu, "Kerr-lens mode-locked femtosecond Cr^{2+}:ZnSe laser at 2420 nm", Optics Letters 2009. **34**: p3056-3058.

- **Huseyin Cankaya**, James G. Fujimoto, Alphan Sennaroglu, “Low-threshold, 12-MHz, multipass-cavity femtosecond Cr^{4+}:forsterite laser”, Laser Physics, 2009. **19**: p.281-284.
- Hamit Kalaycioglu, **Huseyin Cankaya**, Gonul Ozen, M. Lutfu Ovecoglu, Alphan Sennaroglu, “Lasing at 1065 nm in bulk Nd^{3+}-doped tellurite-tungstate glass“, Optics Communications, 2008. **281**: p.6056-6060.
- Hamit Kalaycıoğlu, **Huseyin Cankaya**, M. Natali Cizmeciyan, Alphan Sennnaroglu, Gonul Ozen, “Spectroscopic Investigation of Tm^{3+}:TeO_2-WO_3 glass”, Journal of Luminescence, 2008. **128**: p.1501-1506.
- **Huseyin Cankaya**, Umit Demirbas, Ahmet K. Erdamar, Alphan Sennaroglu, “Absorption saturation analysis of Cr^{2+}:ZnSe and Fe^{2+}:ZnSe”, Journal of Optical Society of America B, 2008. **25**: p.794-800
- Alper Kiraz, S.Cigdem Yavuz, Yasin Karadag, Adnan Kurt, Alphan Sennaroglu, and **Huseyin Cankaya**, “Large spectral tuning of liquid microdroplets standing on a superhydrophobic surface using optical scattering force”, Applied Physics Letters, 2007. **91**: p. 231102.
- Alphan Sennaroglu, **Huseyin Cankaya**, Adnan Kurt “Repetition Rate Control in Continuous-Wave Pumped Passively Q-switched Solid-State Lasers ”, Optical Engineering, 2007. **46:** p. 24201.

MANUSCRIPT UNDER REVISION

- **Huseyin Cankaya**, M. Natali Cizmeciyan, Ersen Beyatli, Adil Tolga Gorgulu, Adnan Kurt and Alphan Sennaroglu "Efficient injection-seeded gain-switched tunable Cr:ZnSe laser" Optics Letters (submitted).
- M. Natali Cizmeciyan, **Huseyin Cankaya**, Adnan Kurt and Alphan Sennaroglu "Operation of femtosecond Kerr lens mode-locked Cr:ZnSe lasers with different dispersion compensation methods" Applied Physics B (submitted).

CONFERENCE PROCEEDINGS

- Adil Tolga Gorgulu, **Huseyin Cankaya**, Adnan Kurt, Adolfo Speghini, Marco Bettinelli, and Alphan Sennaroglu, "Spectroscopic investigation of Tm^{3+}:TeO_2 -K_2O-Nb_2O_5 glasses at different doping levels for 2 μm laser applications", Advances in Optical Materials (Istanbul, Turkey, February 16-18, 2011)
- M. Natali Cizmeciyan, **Huseyin Cankaya**, Adnan Kurt and Alphan Sennaroglu "Dispersion compensation schemes for femtosecond Kerr-lens mode-locked Cr:ZnSe lasers" ASSP 2011, Istanbul, Turkey.
- **Huseyin Cankaya**, James G. Fujimoto, Alphan Sennaroglu, "80-nJ multipass-cavity chirped-pulse Cr^{4+}:forsterite laser", Advanced Solid-State Photonics (San Diego, California, USA, January 31-February 04, 2010)

- **Huseyin Cankaya** and Alphan Sennaroglu, "Nd^{3+}-Doped Tellurite Glass Laser at 1.37 μm", IEEE LEOS (Antalya, Turkey, October 04-08, 2009)
- **Huseyin Cankaya**, James G. Fujimoto and Alphan Sennaroglu "Efficient low-threshold multipass-cavity femtosecond Cr^{4+}:forsterite laser" ASSP 2009, Denver, Colorado, USA.
- **Huseyin Cankaya**, James G. Fujimoto, Alphan Sennaroglu, "Low-threshold, Multipass-cavity, Femtosecond Cr^{4+}:forsterite laser", 17^{th} International Laser Physics Workshop (Trondheim, Norway, June 30-July 04, 2008)
- Hamit Kalaycioglu, **Huseyin Cankaya**, Gonul Ozen, M.Lutfu Ovecoglu, Alphan Sennaroglu, "Laser action in bulk Nd^{3+}-doped telluride glass", CLEO (San Jose, USA, May 04-09, 2008)